

Review

Small molecular gadolinium(III) complexes as MRI contrast agents for diagnostic imaging

Kannie Wai-Yan Chan, Wing-Tak Wong*

Department of Chemistry, The University of Hong Kong, Pokfulam Road, Hong Kong, China

Received 17 October 2006; accepted 26 April 2007

Available online 3 May 2007

Contents

1. Introduction	2429
2. Contrast agent architectures and relaxivity	2431
2.1. Clinical contrast agents	2431
2.2. New contrast agents in the millennium	2431
2.2.1. Cyclic polyaminocarboxylate chelates	2431
2.2.2. Acyclic polyaminocarboxylate chelates	2436
3. Pharmacokinetics	2441
3.1. HSA binding	2442
3.2. Relaxivity of HSA adducts	2442
3.3. Macromolecular structures	2443
4. Biomedical applications	2444
4.1. Blood-pool agents	2444
4.2. Hepatobiliary and renal agents	2445
4.3. Molecular agents	2446
5. Conclusions	2448
Acknowledgements	2448
References	2448

Abstract

Magnetic resonance imaging (MRI) contrast agents that contain the gadolinium ion are widely used in biomedical research and diagnosis. The relaxation mechanism of these T_1 -agents highlights their sensitivity towards the proximal environment. Greater knowledge of the structurally related relaxation mechanism, particularly factors that govern relaxivity, leads to scrutinized chelate designs that improve contrast enhancement. Cyclic and acyclic polyaminocarboxylate gadolinium complexes, especially those have favourable water exchange and tumbling rate for relaxation, have been reported to improve relaxivity and specificity.

The criteria for a large relaxivity gain upon protein binding, such as the human serum albumin (HSA), are elucidated through the relaxometric study of the protein–chelate adduct. This adduct is an important model for the development of contrast agents, which may allow the in vivo visualization of proteins. The strength of HSA binding and the observed relaxivity are related to the pharmacokinetic profile of the contrast agents and give insight in the sensitivity of the agents after intravenous administration. By using animal models, an understanding of the physiology of contrast agents, including their biodistribution, excretion, and possible site of interaction, is acquired. The in vitro studies of contrast agents have demonstrated the feasibility of imaging various disease-related proteins, cell types, and gene delivery and expression. Imaging at the molecular level can be achieved through this integrative approach and the incorporation of nanotechnology in drug delivery.

© 2007 Elsevier B.V. All rights reserved.

Keywords: MRI contrast agents; Gadolinium(III) complexes; Molecular imaging; Protein probes; Polyaminocarboxylates

* Corresponding author. Tel.: +852 28592157.

E-mail address: wtwong@hkucc.hku.hk (W.-T. Wong).

1. Introduction

The superior spatial resolution of contrast-enhanced magnetic resonance imaging (MRI) and advances in proteomics and genomics have revolutionized the medical imaging field. High field scanners have a short scanning time and have improved both signal-to-noise (SNR) and contrast-to-noise (CNR) ratios. The resolution can be optimized to the tenths of μm . The availability of specific and “smart” contrast agents in frontier research has a major contribution to the success of molecular imaging. ‘Smart’ contrast agents are agents that response to the pathological or physiological parameters, such as pH, temperature, partial oxygen pressure $p\text{O}_2$, metal ions [1] or the concentration of enzymes. In 2000, Meade et al. reported the first “smart” contrast agent that shows a significant change in the relaxivity *in vivo* in the presence of an enzymatic cleavable bond. This is a breakthrough in the development of small molecular Gd-based agents, which uses EgadMe to probe the enzyme mRNA expression and visualize the reporter gene expression in *X. laevis* embryos [2].

Image contrast has improved greatly in the presence of contrast agents, and with a better knowledge of the structurally related relaxation mechanism. It is governed by three parameters: proton density, longitudinal relaxation time T_1 ; and transverse relaxation time T_2 . The variation in the proton density between tissues is small; therefore, the pulse sequence that measures the T_1 and T_2 provides the necessary contrast for diagnosis. Two categories of contrast agents are available to alter the relaxation rate in the tissues where they distributed, and are named the T_1 -agent and the T_2 -agent. The T_1 -agent, which is commonly the gadolinium complex, reduces the longitudinal relaxation time and gives a positive contrast. The iron oxide is a T_2 -agent, which results in a negative contrast. The use of these contrast agents improves both the sensitivity and specificity of MRI, and provides anatomical and physiological information.

Gd-based T_1 -agents modify the longitudinal relaxation. By ascertaining this relaxation, contrast agents can be designed

precisely to increase relaxivity. The origin of relaxation is the dipole-dipole interactions between the proton nuclear spins and the fluctuating local magnetic field that results from the paramagnetic metal center. The water molecules that are coordinated with the metal center make a direct contribution, and the bulk solvent molecules experience the paramagnetic effect when they diffuse around the metal center. These two interactions are the major constituents of the observed relaxivity (as stated in Eq. (1.1)) and are known as the inner-sphere relaxation rate and outer-sphere relaxation rate, respectively. In addition, water molecules may be retained in the periphery of the metal center through hydrogen bonding for a relatively long time without binding to the metal, which is known as the second-sphere relaxation. This contribution plays a significant role in polyaminocarboxylic chelates [3], especially those with phosphonate groups. Fig. 1 shows the graphical representation of the components in the longitudinal relaxation:

$$R_1^{\text{obs}} = R_{1p}^{\text{IS}} + R_{1p}^{\text{OS}} + R_1^{\text{W}}, \quad (1.1)$$

where R_{1p}^{IS} and R_{1p}^{OS} are the relaxation enhancement in the presence of the paramagnetic complex at 1 mM concentration, R_1^{obs} is the overall measured relaxivity and R_1^{W} is the relaxation rate of the solvent in the absence of the paramagnetic complex.

Relaxivity describes the efficacy of the paramagnetic contrast agent in changing the rate of water proton relaxation at 1 mM concentration. The contrast enhancement of Gd complexes on T_1 is shown in Eq. (1.2). The microscopic paramagnetic relaxation that contributes to T_1 is modulated by the water exchange rate, the reorientation of the whole complex and the electron spin relaxation. Their relationship is expressed by the modified Solomon–Bloembergen equations (Eqs. (1.3)–(1.5)). The effectiveness of paramagnetism decreases as the radial distance increases because the dipolar interaction decreases. Therefore, the mechanism that brings water molecules to the proximity of the gadolinium ion through the exchange between the bound water molecules and those in peripheral is important in the propagation of the paramagnetic effect. The water exchange can be

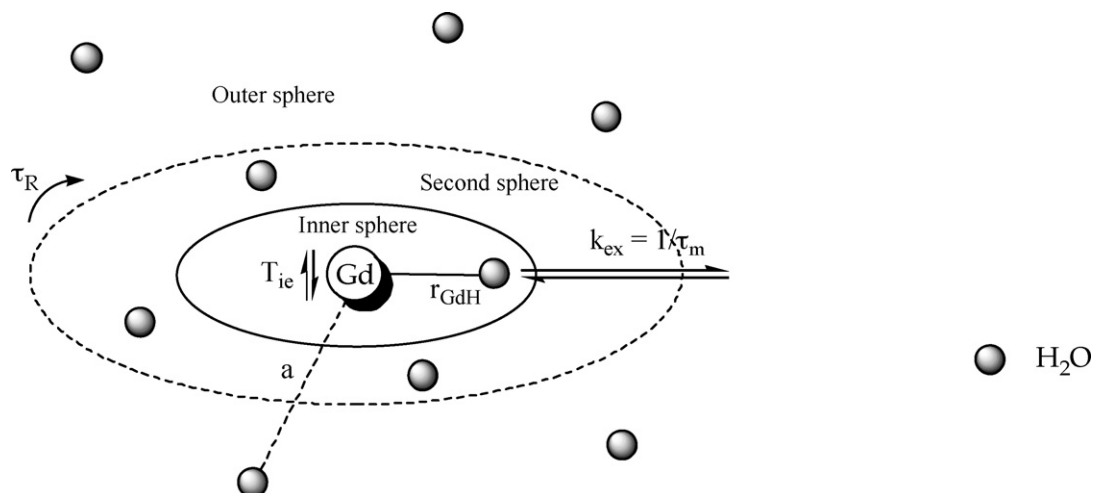


Fig. 1. Diagram shows the parameters of the longitudinal relaxivity.

subdivided into the prototropic exchange and the water exchange [4]:

$$R_{1p}^{IS} = \frac{1}{T_1} = \frac{[M]q}{55.6(T_{1M} + \tau_m)}, \quad (1.2)$$

$$\frac{1}{T_{1M}} = \frac{1}{T_1^{DD}} + \frac{1}{T_1^{SC}}, \quad (1.3)$$

$$\frac{1}{T_1^{DD}} = \frac{2}{15} \left[\frac{\gamma_I^2 g^2 \mu_B^2 S(S+1)}{r_{GdH}^6} \right] \left(\frac{\mu_0}{4\pi} \right)^2 \times \left(\frac{7\tau_{c2}}{1 + \omega_s^2 \tau_{c2}^2} + \frac{3\tau_{c1}}{1 + \omega_I^2 \tau_{c1}^2} \right), \quad (1.4)$$

$$\frac{1}{T_1^{SC}} = \frac{2S(S+1)}{3} \left(\frac{A}{\hbar} \right)^2 \left(\frac{\tau_{c2}}{1 + \omega_s^2 \tau_{c2}^2} \right), \quad (1.5)$$

where $[M]$ is the molar concentration of paramagnetic ions, q the hydration number per Gd center, τ_m the residence lifetime of inner-sphere water molecules, $1/T_{1M}$ the longitudinal proton relaxation rates, γ_I the nuclear gyromagnetic ratio ($\gamma(H) = 42.6 \text{ MHz/T}$), S is $7/2$ for Gd ions, g the electron g -factor, μ_B the Bohr magneton, r_{GdH} the electron spin–proton distance, ω_I and ω_s are the nuclear and electron Larmor frequencies, respectively, and A/\hbar is the hyperfine or scalar coupling constant between the electron spins of the paramagnetic center and the proton spins of the coordinated water molecule. The correlation times have a relationship, as stated in Eqs. (1.6) and (1.7), where τ_R is the rotational correlation time, and T_{1e} is the longitudinal electron spin relaxation time of the metal ion:

$$\frac{1}{\tau_{c1}} = \frac{1}{\tau_R} + \frac{1}{T_{1e}} + \frac{1}{\tau_m} \quad (1.6)$$

$$\frac{1}{\tau_{e1}} = \frac{1}{T_{1e}} + \frac{1}{\tau_m}, \quad (1.7)$$

The interdependence of these parameters is complicated by the effect of magnetic field strength. The typical field strength of clinical MRI scanners is 1.5 or 3 T, and the highest field strength for the human and animal scanner is 9.4 T and higher than 14 T, respectively [5].

Structural modifications on ligands improve the above parameters of T_1 relaxation and lead to a higher relaxivity with respect to the traditional contrast agents [6–9]. Ligands occupy seven coordination sites of Gd ions and form diaqua complexes is preferred. This may increase the relaxivity directly and maintain a stable chelation. Estimation shows that a decrease of 0.2 \AA of the distance r_{GdH} between the coordinated water and Gd leads to a 50% increase in inner-sphere relaxivity [6,10], because the relaxivity has a sixth-order dependence on the distance, as expressed in Eq. (1.4). A slow water exchange rate ($k_{ex} = 1/\tau_m$) may limit the relaxation enhancement of the T_1 -agents, especially for diethylenetriaminepentaacetic acid (DTPA) or 1,4,7,10-tetraazacyclododecane- N,N',N'',N''' -tetraacetic acid (DOTA) types of complexes, which have k_{ex} smaller than 10^6 s^{-1} [7].

A dissociative water exchange mechanism is adopted by complexes having an octadentate chelate with one inner-sphere water molecule. A detailed exchange mechanism of trivalent lanthanide complexes is described by Merbach et al. [11]. There are two distinctive situations as predicted by Eqs. (1.3)–(1.7). One is a slow water exchange ($T_{1M} \ll \tau_m$) in which the residence lifetime τ_m is the dominant factor, whereas the other one is a fast water exchange ($T_{1M} \gg \tau_m$), and its relaxivity is a dependent of the proton exchange and the rotation and electronic relaxation. The tuning of the steric environment in the vicinity of the Gd centre can increase the dissociative water exchange rate as well as the increase relaxivity. An increase in the water exchange rate can be achieved by increasing the portion of a particular isomer that has a shorter τ_m , and the optimal value of τ_m is 30 ns at 20 MHz. Another factor that limits the relaxivity is the reorientational correlation time τ_R . Strategies are employed to lengthen τ_R from a typical range of 50–90 ps to hundreds of picosecond. The formation of covalently or noncovalently bound macromolecules [8], such as dendrimers [12] or linear polymers [13] or proteins [14], can efficiently retard the rotational motion of the complex and increase τ_R . Alternatives are micellar self-assembly [15] and incorporated liposomes [16]. When these parameters including the water exchange rate, rotation and electron paramagnetic relaxation are optimized, the maximum relaxivity predicted by Solomon-Bloembergen-Morgan theory can reach $100 \text{ mM}^{-1} \text{ s}^{-1}$ for a complex with $q = 1$ at 20 MHz [9].

Another important issue in the contrast agent development is safety. The first Gd-based MRI contrast agent, $[\text{Gd-DTPA}(\text{H}_2\text{O})]^{2-}$ MagnevistTM, was reported in 1981, and numerous molecular designs emerged in the following two decades. The high spin state and long electronic relaxation time make Gd a good candidate. However, the free Gd ion accumulates in the liver, spleen, and bones, and is highly toxic, with a $\text{LD}_{50} \sim 0.2 \text{ mmol kg}^{-1}$ in mice [17,18]. Therefore, chelates are designed to form complexes with Gd and to minimize the toxicity to a biologically tolerable level of $\text{LD}_{50} \sim 10 \text{ mmol kg}^{-1}$. Complexes should be both thermodynamically [18] and kinetically stable, which is secured by the preorganization effect of a cyclic chelate, such as $[\text{Gd-DOTA}(\text{H}_2\text{O})]^-$ DotaremTM. The transmetallation of gadolinium with endogenous metal ions such as copper and zinc is less common in cyclic chelates than acyclic chelates [19]. For the clinical agents, the LD_{50} falls into a range of 8–15 mmol kg^{-1} [20–22], and reported adverse effects for these Gd-based contrast agents are rare [23–25].

Macromolecular contrast agents, such as nanoparticles, dendrimers, peptides, antibodies, and proteins, have a high relaxivity relative to the traditional contrast agents, but their size prevents effective extravasation from the vasculature. The consequence is a reduction in the diffusion through the interstitium, which affects cellular delivery. They demonstrate a wide range of possibilities in molecular imaging; however, their preparations are neither cost – nor time – effective, their shelf life is limited, and they possess potential immunogenicity [26]. Small molecular contrast agents, which have promising targeting ability, diffusion and penetration and relaxivity that can be modified according to different physiological states, have a crucial role in the imaging

field. However, the relaxivity of these agents is limited; hence methods have to be employed to increase their sensitivity. After assessing different potential molecular architectures, the development of contrast agents is accentuated to the small molecular Gd-based agent [1,27].

In this review, advances in the millennium in this multi-disciplinary research are addressed. New agents aim to improve the relaxivity and specificity, which specificity describes the selectivity of the contrast agent for a particular target, of clinical agents. Structural modifications of the coordinating environment around the Gd will be used to elucidate the effectiveness of a reduced τ_M or a lengthened τ_R in increasing relaxivity. The mechanistic study of the reversible non-covalent binding of contrast agents with human serum albumin (HSA) is one of the protein–chelate interactions that show an increase in relaxivity. Moreover, this interaction demonstrates the pharmacokinetics of contrast agents after intravenous injection, which reflects the availability of the agents in the intra- and extra-vascular compartments. Criteria for the blood-pool, hepatobiliary and renal agents and the efficacy of these agents *in vivo* are discussed. Strategies that are based on biomolecular interactions have been devised to image at molecular level, illustrating the indispensable role of contrast agents in molecular imaging. This comprehensive approach of analyzing the physiochemistry and pharmacokinetics assists the understanding of possible advantages or limitations in diagnosis, and may catalyze the process of moving contrast agents from the research arena to clinical applications.

2. Contrast agent architectures and relaxivity

2.1. Clinical contrast agents

The clinical T_1 -agents have a molecular weight around 600 Da and relaxivities between 4 and 5 mM^{−1} s^{−1} at 20 MHz and 310 K, as shown in Table 1. They are regarded as nonspecific agents or extracellular fluid space (EFS) agents, except MultiHanceTM and EovistTM, which are hepatobiliary agents. The EFS agents are mainly distributed in the intravascular and interstitial spaces, and are excreted by the glomerular filtration in the kidneys. Hepatobiliary agents have affinity towards HSA and are specifically uptaken by the hepatocytes. They are partially excreted through the biliary system and the kidneys. By comparing the structure of hepatic agents with that of EFS agents, the liver specificity can be ascribed to the pendent hydrophobic phenyl rings.

Acyclic DTPA and cyclic DOTA are two common skeletons of gadolinium chelates. These polyaminocarboxylate ligands control the steric and electronic properties of the Gd complex, that is, the steric environment around the water exchange site [28] and the basicity of the pendent group on the amine [29]. The OmniscanTM and OptiMarkTM are modified based on MagnevistTM with the aim to increase the hydrophobicity and reduce the osmotic load via intravenous injection. However, the water exchange rate decreases dramatically and casts a major limitation on a high relaxivity. The τ_m varies between 80 and 970 ns at 298–310 K, which is far from the optimum

value. Both MultiHanceTM and EovistTM have a faster water exchange rate ($k_{ex} = 7.0 \times 10^6$ s^{−1}) and a shorter r_{GDH} [10] than those of MagnevistTM because of a more steric environment for water exchange. Therefore, two agents have a higher observed relaxivity.

To cope with the surging demand for contrast agents in molecular imaging, tailor-made chelates are required to improve relaxivity through the modulation of the coordination environment around the Gd center and, at the same time, to serve as specific agents for the *in vivo* micro-environment.

2.2. New contrast agents in the millennium

2.2.1. Cyclic polyaminocarboxylate chelates

Researchers are trying to create new agents with higher relaxivity, and numerous Gd-based cyclic agents have been reported (as summarized in Table 2). The structural relationship of the relaxivity to different influencing parameters, such as water exchange rate, electronic effect and reorientational correlation time τ_R is highlighted.

Efforts have been devoted to decreasing the residence lifetime τ_m of complexes, which is a limiting factor for obtaining a high relaxivity. Water exchange rates depend on different steric environments around the Gd centre in different isomers. The conformation and coordination of DOTMA [35,36] and DOTA with different lanthanide(III) have been studied [37,38]. The square antiprism-SAP (M or $\Delta(\lambda\lambda\lambda\lambda)/\Lambda(\delta\delta\delta\delta)$) and twisted square antiprism-TSAP (m or $\Delta(\delta\delta\delta\delta)/\Lambda(\lambda\lambda\lambda\lambda)$) isomers are found in the cyclen system. The TSAP is expected to have a faster water exchange rate due to a more sterically crowded coordination environment, which has a torsion angle that is 10° smaller than that of the SAP isomer. Complexes **29** and **42** have SAP and TSAP as the dominant isomer, respectively. The exchange rate of the TSAP isomer reaches $k_{ex} = 67 \times 10^6$ s^{−1} for 2-*p*-nitrobenzyl-DOTMA, which is an order of magnitude faster than its SAP isomer of $k_{ex} = 8.3 \times 10^6$ s^{−1} [39]. This phenomenon was also found in a series of tetrasubstituted cyclen that was reported by Merbach et al. [40], which showed the importance of *m/M* ratio in the τ_m of these complexes. Sherry et al. presented two Gd-DOTA-bis(amide) complexes [41] in which the water exchange rate of the SAP isomer resembled that of the Gd-DOTA-like complexes. However, the steric compression around the water binding site increases the water exchange rate of the TSAP isomer. The exchange rate is enhanced if TSAP is the dominant species in the solution, thus forming a favourable *m/M* ratio [42]. This monophosphonate derivative has a pH dependent water exchange, which the exchange rate increases as the pH increases.

The steric crowding can also be modulated by the introduction of a linker, such as methylene between the annular amine and the pendent amide groups [43]. The complex having this linker has a fast water exchange rate of $k_{ex} = 111.1 \times 10^6$ s^{−1}. If the methylene group is added between the amines on cyclen, such as the TRITA type complexes, an increase in the water exchange is observed due to the sterically compressed water exchange site [44]. Complexes **51** and **52** are 2,2'-bipyridine containing cryptand ligands. They are positively charged and have a slow water exchange rate. Unlike the clinical agents,

Table 1
Selected relaxometric parameters of clinical contrast agents

Complex/generic name (common name)	Ligand structure	MW	r_1/r_1^* ($\text{mM}^{-1} \text{s}^{-1}$) (20 MHz/310 K)	τ_m (ns) (310 K)	τ_R (ps) (310 K)	τ_V (ps) (310 K)	Reference
$[\text{Gd}(\text{H}_2\text{O})_8]^{3+}$			11.0 (298 K; 400 MHz)	1.2 (298 K)	41 (298 K)	7.3 (298 K)	[30]
1 $[\text{Gd-DTPA}(\text{H}_2\text{O})]^{2-}$ /Magnevist (gadopentetate dimeglumine) ^a		547	3.8/4.9	143	54	25	[25,31]
2 $[\text{Gd-DTPA-BMA}(\text{H}_2\text{O})]$ /Omniscan (gadodiamide) ^a		573	3.8/4.8	967	65	18	[5,31]
3 $[\text{Gd-DTPA-BMEA}(\text{H}_2\text{O})]$ /OptiMARK (gadoversetamide)		661	4.1 (308 K)	1320 (308 K)	71 (308 K)	35 (308 K)	[32]
4 $[\text{Gd-BOPTA}(\text{H}_2\text{O})]^{2-}$ /MultiHance (gadobenate dimeglumine) ^a		711	4.8/9.7	140	89	30	[25,31]
5 $[\text{Gd-EOB-DTPA}(\text{H}_2\text{O})]^{2-}$ /Eovist (gadoxetate)		682	5.5	82	86	28	[33,34]
6 $[\text{Gd-DOTA}(\text{H}_2\text{O})]^-$ /Dotarem (gadoterate meglumine) ^a		558	3.5/4.3	122	53	7	[25,31]
7 $[\text{Gd-HPDO3A}(\text{H}_2\text{O})]$ /ProHance (gadoteridol) ^a		558	3.6/4.6	217	51	7.5	[25,31]
8 $[\text{Gd-DO3A-butrol}(\text{H}_2\text{O})]$ /Gadovist (gadobutrol) ^a		604	3.7/5.6	176	57	6.5	[25,31]

r_1^* : relaxivity in plasma; MW: molecular weight; NA: not available.

^a r_{GdH} fixed at 3.1 Å.

Table 2
Gadolinium complexes of cyclic polyaminocarboxylate

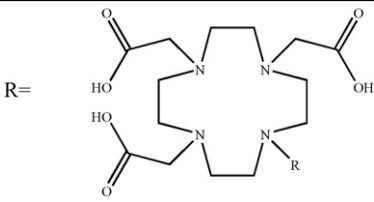
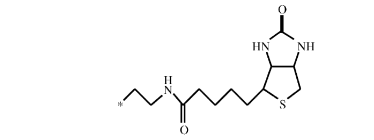
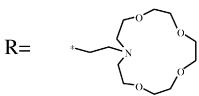
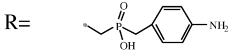
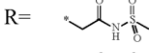
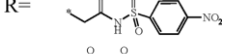
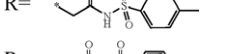
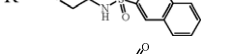
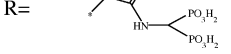
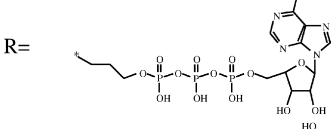
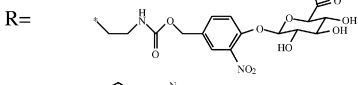
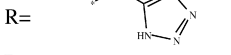
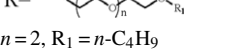
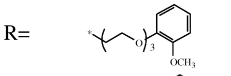
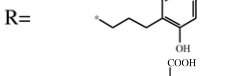
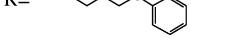
Complex	Ligand structure	MW	q	r_1 (mM ⁻¹ s ⁻¹) (20 MHz/298 K)	τ_m (ns) (298 K)	τ_R (ps) (298 K)	Reference
9		599	NA	3.3 (300 MHz)	NA	NA	[47]
10		777	NA	5.4 (300 MHz)	NA	NA	[47]
11	R = CH ₂ CONH(CH ₂) ₃ SH	477	NA	2.9 (200 MHz, 310 K)	NA	NA	[48]
12	R = CH ₂ CONH(CH ₂) ₆ SH	519	NA	2.3 (200 MHz, 310 K)	NA	NA	[48]
13		591	2	9.5	32	NA	[49]
14	R = CH ₂ CH ₂ NH ₃ ⁺	390	2	5.9	240	NA	[49]
15		529	1	6.7 (10 MHz)	16	88	[50]
16		480	1	4.5	507	NA	[51]
17		587	1	5.0	746	NA	[51]
18		556	1	5.1	613	NA	[51]
19		592	1	5.3	NA	NA	[51]
20		577	1	5.3	1180	88	[52]
21		893	2	6.5 (24 MHz, 308 K)	NA	NA	[53]
22		760	1	3.9 (60 MHz, 310 K)	NA	NA	[54]
23		428	1	4.8	NA		[55]
24		534	1	3.9	180	90	[56]
25	$n = 6$, R ₁ = CH ₃	684	1	4.6	216	86	[56]
26		584	1	4.1	500	85	[56]
27		480	2	7.4	770	120	[56]
28		524	2	7.5	18	116	[56]

Table 2 (Continued)

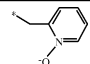
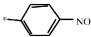
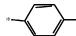
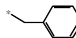
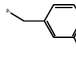
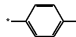
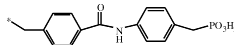
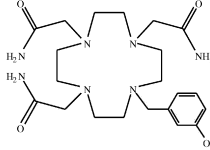
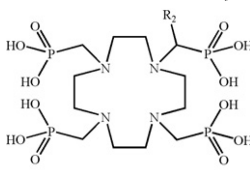
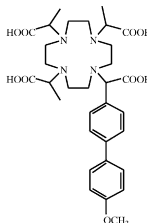
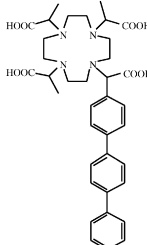
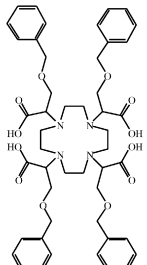

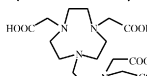
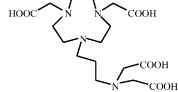
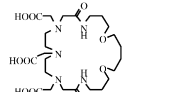
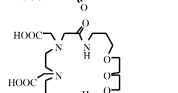
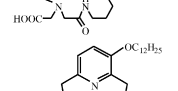
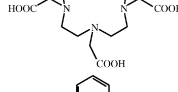
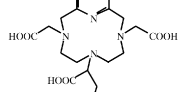
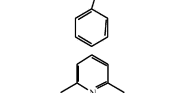
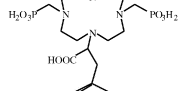
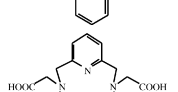
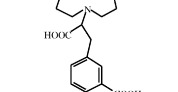
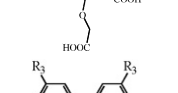
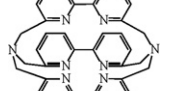
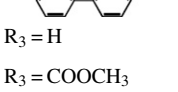
Complex	Ligand structure	MW	q	r_1 (mM ⁻¹ s ⁻¹) (20 MHz/298 K)	τ_m (ns) (298 K)	τ_R (ps) (298 K)	Reference
29	R= 	453	1	4.1(310 K)	39	NA	[57]
30	R= 	467	2	8.0 (10 MHz)	135	77	[29]
31		437	2	8.5 (10 MHz)	57	81	[29]
32		515	2	10.5 (10 MHz)	46	NA	[58]
33		466	2	9.5 (10 MHz)	32	Na	[58]
34		515	2	7.5	15	102	[59]
35		649	2	11.0	12	161	[59]
36		463	2	9.0 (10 MHz)	99	NA	[58]
37		660	0	5.1	NA	NA	[45]
38	R ₂ = (CH ₂) ₇ CH ₃ R ₂ = (CH ₂) ₁₀ CH ₃	702	0	4.6	NA	NA	[45]
39		628	NA	6.0	65	NA	[60]
40		674	NA	6.4	NA	NA	[60]
41		884	1	8.7	NA	NA	[61]
42		404	1	3.9	53	73	[62]
43		404	1	4.8 (61 MHz)	NA	NA	[63]

Table 2 (Continued)

Complex	Ligand structure	MW	q	r_1 (mM ⁻¹ s ⁻¹) (20 MHz/298 K)	τ_m (ns) (298 K)	τ_R (ps) (298 K)	Reference
44		418	1	4.7 (61 MHz)	NA	NA	[63]
45		561	1	5.9	1100	110	[64]
46		577	1	6.1	1500	121	[64]
47		564	2	13.5	70	473	[65]
48		471	2	8.3	58	92	[66]
49		543	1	8.1	75	120	[66]
50		589	2	10.5	79	134	[66]
51		574	3	9.8	556	88	[67]
52		690	3	11.2	1031	108	[67]
53		1098	2	4.1 per Gd	53	183	[68]
54		832	2	3.6 per Gd (310 K)	769	150	[69]
55		886	2	6.25 per Gd (310 K)	910	130	[69]
56		1148	8	19.4 (24 MHz, 308 K)	NA	NA	[70]

MW: molecular weight; *: anchoring point. Ph: phenyl ring; NA: not available.

the exchange mechanism is associative because of their unique coordination. Complex **52** has an ester group to retain the inner-sphere water molecule, which is favourable for the associative exchange. Thus, its exchange rate is slower than that of complex **51** and its relaxivity is higher.

Complexes **45** and **46** possess a slow water exchange, and their relaxivities are approximately $6 \text{ mM}^{-1} \text{ s}^{-1}$ and slightly higher than ESF agents. This is probably due to the contribution of the second-sphere water molecules in the presence of the ether-linked annular oxygen. Although direct evidence for second-sphere relaxation is difficult to obtain, the hydrogen-bond water molecules cannot be neglected [3]. The second hydration sphere has a significant role in complexes without inner-sphere water molecules, e.g. Gd-DOTP [3]. Complexes **37** and **38** are DOTP analogues without inner-sphere water molecules. The presence of the phosphonate groups help to attract water molecules to the second-sphere, therefore enhances the relaxivity [45]. A phosphonate group is added on the Gd-PCTA-[12] to increase the second-sphere interaction [46].

The electronic effect contributes to the modulation of the water exchange rate, such as the basicity of the amine on the cyclen. Several complexes that were studied by Aime et al. (complexes **30** and **31**) show that the positive inductive effect on the aromatic ring favours a faster water exchange rate because of the destabilization of the Gd–O bond of the bound water molecule. The lability of the coordinated water is particularly interested in the case of the DO3 A-like chelate, which has a nine coordinated ground state and a dissociative water exchange [30]. On contrary, the delocalization of the negative charge on complexes **16–18** through the *N*-sulfonylacetamide decreases the water exchange rate.

The short reorientational correlation time τ_R of small molecular gadolinium agents is another factor that limits the relaxivity. Complex **15** has an optimal water exchange rate because the TSAP and SAP isomers have similar τ_m . However, the relaxivity increase is limited by the reorientational correlation time τ_R , which is assessed by the ^{17}O longitudinal relaxation of the complex in solution. Dimeric and tetrameric ligands, such as complexes **53–56**, have a longer τ_R than the monomeric ligands. Complex **53** has a longer τ_R than complex **54** due to the presence of the phenyl rigid linker, reducing the flexibility between the two Gd centers. Lipophilicity favours the intermolecular interaction of complex **47**. This slows down the tumbling rate of the complex and results in a higher relaxivity than the Gd-PCTA-[12], which is a complex without the C_{12} carbon side chain. The combination of these factors has a favourable Gd coordination for a fast water exchange.

2.2.2. Acyclic polyaminocarboxylate chelates

The majority of Gd complexes in the acyclic family (see Table 3) are DTPA derivatives with functional moieties such as amide and phenyl. The steric environment and the number of coordinated water molecules influence relaxivity. Their relaxivities fall in the range of $3.6\text{--}7.2 \text{ mM}^{-1} \text{ s}^{-1}$. The τ_m are relatively long in μs range, especially in chelates that are less sterically hindered and do not have a negative charge. The stereoisomers of complexes **84** and **85** have a similar τ_m with a similar

steric environment. A long aliphatic substituent on the nitrogen may increase the hydrophobicity around Gd and increase the water exchange rate under a dissociative exchange. Muller et al. [71] prepared a series of DTPA bisamide complexes **68–73** that showed a reduction in residence lifetime as the alkyl chain length increased. On the other hand, the bulky butyl groups on the amide nitrogen of complexes **59** and **60** reduce the water exchange rate to a very slow level of $k_{\text{ex}} = 0.6 \times 10^6 \text{ s}^{-1}$ with a lower negative charge and reduced steric hindrance. This is a result of the less dissociative water exchange, and the fact that the butyl group prevents the incoming water molecules from participating in the exchange process. For the triamide derivative, such as complex **59**, the absence of the acetate group may stabilize the eight-coordinated transition state in the exchange process, which results in a slower exchange of the bound water molecules [72]. Moreover, the substitution in complex **59** of the third acetate group by an amide group has a less pronounced effect on a decrease in the water exchange rate relative to complex **60**.

The substituent on the first carbon has a significant effect on the hydration shell, particularly on the nitrogen of the amine group. The butyl groups in complexes **77** and **78** demonstrate that only a hindrance on the first carbon can effectively increase the water exchange rate. The modification on the α -carbon on the nitrogen by a phenyl group further decreases the τ_m value of the DTPA-like complex **84–87** ns. The DTPA skeleton was modified to TTDA by changing the ethylene to propylene. TTDA derivatives like complexes **90–96** have an additional steric strain which leads to faster water exchange rates (the τ_m decreases to a few nanoseconds) than that of a DTPA complex. This effect prevails and is significant in monoaqua nine-coordinated Gd complexes that have a dissociative water exchange. The most prominent change of τ_m is in Gd-EPTPA ($\tau_m = 3 \text{ ns}$) which is almost two order of magnitude faster than that of Gd-DTPA [73]. Further modifications on the side arm turn the pendent ethylene group to propionate such as Gd-DTTA-Nprop ($\tau_m = 12.5 \text{ ns}$) [74], and this terminal substitution of the acetate group has a more pronounced effect than the central substitution; or include the phenyl or ethoxybenzyl group like complexes **90–92**, which have short τ_m for a high relaxivity. The relaxivity increases further for complexes that have two inner-sphere water molecules (complexes **93**, **95** and **96**) and a fast water exchange.

There are a number of new polyaminocarboxylate skeletons, such as complexes **97–104**. They are designed to accommodate more than one inner-sphere water molecule and thus increase relaxivity. As demonstrated by Raymond et al. the hydroxypyridonate (HOPO) ligands of complexes **106–118** have intramolecular hydrogen bonds to facilitate the water exchange [75]. The residence lifetime is shortened to one tenth of a nanosecond, and the inner-sphere hydration number increases to two or three. The relaxivities are optimized to $8.8\text{--}11.1 \text{ mM}^{-1} \text{ s}^{-1}$. For the dendrimeric analogue complex **113**, the τ_m is 10 ns, and the τ_R increases to 238 ps, resulting in the highest relaxivity ($14.3 \text{ mM}^{-1} \text{ s}^{-1}$) among the HOPO-type chelates. The pyrimidinone analogue of HOPO, such as Gd-[TrenHOPY], has two inner-sphere water molecules and a faster water exchange rate of $k_{\text{ex}} = 4.9 \times 10^8 \text{ s}^{-1}$ [76]. It has a better solubility than the HOPO complex. Unlike complexes

Table 3
Gadolinium complexes of acyclic polyaminocarboxylate

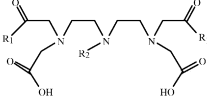
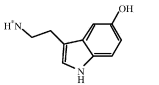
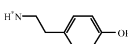
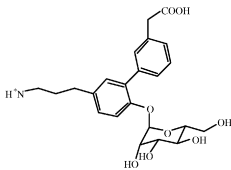
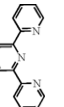
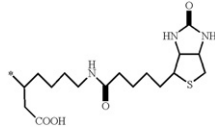
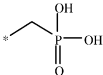
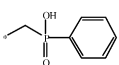
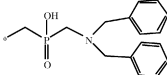
Complex	Ligand structure	MW	q	r_1 (mM ⁻¹ s ⁻¹) (20 MHz/298 K)	τ_m (ns) (298 K)	τ_R (ps) (298 K)	Reference
57	 $R_1 =$  $R_2 = \text{CH}_2\text{COOH}$	709	NA	4.3 (313 K)	NA	NA	[78]
58	$R_1 =$  $R_2 = \text{CH}_2\text{COOH}$	631	NA	4.3 (313 K)	NA	NA	[78]
59	$R_1 = \text{NBu}_2$ $R_2 = \text{CH}_2\text{CONHMe}$	670	1	7.2	1667	293	[72]
60	$R_1 = \text{NBu}_2$ $R_2 = \text{CH}_2\text{COOH}$	657	1	6.8	1020	233	[72]
61	$R_1 =$  $R_2 = \text{CH}_2\text{COOH}$	1167	1	4.6	259 (310 K)	93 (310 K)	[79]
62	$R_1 = \text{OH}$ $R_2 =$ 	566	2	7.3 (313 K)	116	NA	[80]
63	$R_1 = \text{OH}$ $R_2 =$ 	690	NA	6.1 (64 MHz, 293 K)	NA	NA	[81]
64	$R_1 = \text{OH}$ $R_2 =$ 	429	1	5.5	88	86	[82]
65	$R_1 = \text{OH}$ $R_2 =$ 	489	1	5.5	92	110	[82]
66	$R_1 = \text{OH}$ $R_2 =$ 	622	1	5.9	685	121	[82]
67	$R_1 = \text{NH}_2$ $R_2 = \text{CH}_2\text{COOH}$	377	1	3.6 (310 K)	1171 (310 K)	NA	[71]
68	$R_1 = \text{NHCH}_2\text{CH}_3$ $R_2 = \text{CH}_2\text{COOH}$	433	1	3.7 (310 K)	927 (310 K)	NA	[71]
69	$R_1 = \text{NH}(\text{CH}_2)_2\text{CH}_3$ $R_2 = \text{CH}_2\text{COOH}$	461	1	4.0 (310 K)	845 (310 K)	NA	[71]

Table 3 (Continued)

Complex	Ligand structure	MW	<i>q</i>	r_1 (mM ⁻¹ s ⁻¹) (20 MHz/298 K)	τ_m (ns) (298 K)	τ_R (ps) (298 K)	Reference
70	R ₁ = NH(CH ₂) ₃ CH ₃ R ₂ = CH ₂ COOH	489	1	4.4 (310 K)	713 (310 K)	NA	[71]
71	R ₁ = NH(CH ₂) ₄ CH ₃ R ₂ = CH ₂ COOH	517	1	4.3 (310 K)	575 (310 K)	NA	[71]
72	R ₁ = NH(CH ₂) ₅ CH ₃ R ₂ = CH ₂ COOH	545	1	4.5 (310 K)	681 (310 K)	NA	[71]
73	R ₁ = NH(CH ₂) ₆ CH ₃ R ₂ = CH ₂ COOH	573	1	4.5 (310 K)	673 (310 K)	NA	[71]
74	R ₁ = N(CH ₃) ₂ R ₂ = CH ₂ COOH	433	1	3.8 (310 K)	624 (310 K)	NA	[71]
75	R ₁ = N(CH ₂ CH ₃) ₂ R ₂ = CH ₂ COOH	489	1	3.9 (310 K)	654 (310 K)	NA	[71]
76	R ₁ = N(CH ₂ CH ₂ CH ₃) ₂ R ₂ = CH ₂ COOH	545	1	4.5 (310 K)	672 (310 K)	NA	[71]
77	R ₁ = NHC(CH ₃) ₃ R ₂ = CH ₂ COOH	489	1	4.1 (310 K)	654 (310 K)	NA	[71]
78	R ₁ = NHCH(CH ₃) ₂ R ₂ = CH ₂ COOH	461	1	4.2 (310 K)	659 (310 K)	NA	[71]
79	R ₁ = NHCH ₂ CH(OH)CH ₃ R ₂ = CH ₂ COOH	493	1	4.5 (310 K)	1128 (310 K)	NA	[71]
80	R ₁ = NHCH ₂ Ph R ₂ = CH ₂ COOH	557	1	4.2 (310 K)	305 (310 K)	70 (310 K)	[83]
81	R ₁ = OCH ₂ Ph R ₂ = CH ₂ COOH	559	1	3.8 (310 K)	134 (310 K)	58 (310 K)	[83]
82	R ₁ = OH R ₂ = 	575	NA	5.0	NA	NA	[84]
83	R ₃ =  R ₄ = CH ₂ COOH R ₅ , R ₆ = H	661	1	6.4 (80 MHz, 308 K)	NA	NA	[85]
84	R ₃ = OH R ₄ = CH ₂ COOH R ₅ = (S)CH ₂ Ph R ₆ = H	483	1	4.8	87	61 (310 K)	[83]
85	R ₃ = OH R ₄ = CH ₂ COOH R ₅ = (R)CH ₂ Ph R ₆ = H	483	1	4.5	108	62 (310 K)	[83]
86	R ₃ = NHCH ₃ R ₄ = CH ₂ COOH R ₅ = (S)CH ₂ PhOC ₂ H ₅ R ₆ = H	553	NA	5.8	976	84	[33]

Table 3 (Continued)

Complex	Ligand structure	MW	q	r_1 (mM ⁻¹ s ⁻¹) (20 MHz/298 K)	τ_m (ns) (298 K)	τ_R (ps) (298 K)	Reference
87		1719	1	7.5 (64 MHz, 293 K)	NA	NA	[86]
88		1595	NA	8.3 (64 MHz, 310 K)	NA	NA	[87]
89		1268	NA	6.8 (310 K)	599 (310 K)	188 (310 K)	[88]
90		527	1	4.4 (310 K)	8.5	119	[89]
91		527	1	4.4 (310 K)	7.6	125	[89]
92		511	1	4.9 (310 K)	2.3 (310 K)	NA	[90]
93		407	2	5.5 (310 K)	6.7	NA	[91]
94		440	1	3.9 (310 K)	12.5	NA	[91]
95		469	2	5.3 (310 K)	7.1	NA	[91]
96		469	2	4.9 (310 K)	9.1	NA	[91]
97		147	2/3	10.0 (300 MHz)	NA	NA	[92]
98		264	2/3	10.8 (300 MHz)	NA	NA	[92]

Table 3 (Continued)

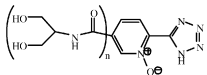
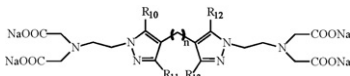
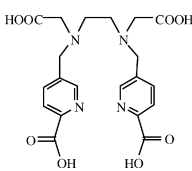
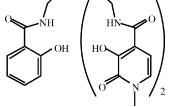
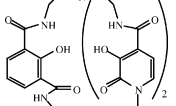
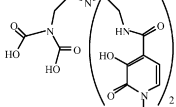
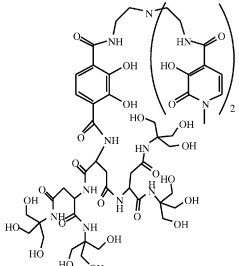
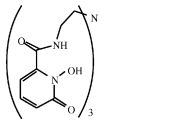
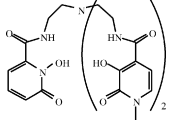
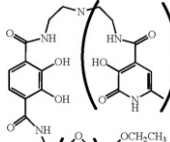
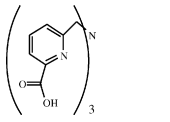
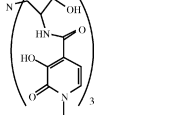
Complex	Ligand structure	MW	q	r_1 (mM ⁻¹ s ⁻¹) (20 MHz/298 K)	τ_m (ns) (298 K)	τ_R (ps) (298 K)	Reference
99		163	2/3	9.3 (300 MHz)	NA	NA	[92]
100	$n=1$	280	2/3	17.7 (300 MHz)	NA	NA	[92]
101		692	4	12.0 (64 MHz, 310 K)	NA	303	[93]
102	$R_{10}=R_{11}=R_{12}=R_{13}=\text{CH}_3$ $n=0$	596	4	14.6 (64 MHz, 310 K)	NA	310	[93]
103	$R_{10}=R_{12}=\text{H}$ $R_{11}=R_{13}=\text{C}_6\text{H}_4\text{-NO}_2\text{-p}$ $n=1$	796	4	18.5 (64 MHz, 310 K)	NA	345	[93]
104	$R_{10}=R_{11}=R_{12}=R_{13}=\text{CH}_3$ $n=1$	610	4	17.7 (64 MHz, 310 K)	NA	370	[93]
105		446	1	5.0	200	55	[94]
106		545	2	7.7	NA	94	[95]
107		602	2	7.2	NA	99	[95]
108		513	1	5.6	NA	110	[95]
109	$R_{14}=\text{CH}_3$	831	2	8.8	8	125	[95]
110	$R_{14}=\text{CH}_2\text{CH}_2\text{NH}_2$	860	2	11.1	2.6	110	[75]
111	$R_{14}=\text{CH}_2\text{CH}_2\text{NHCH}_2\text{CH}_2\text{NH}_2$	903	2	9.7	3.0	114	[75]
112	$R_{14}=\text{CH}_2\text{CH}_2\text{N}(\text{CH}_2\text{CH}_2\text{NH}_2)_2$	946	2	9.0	2.1	127	[75]
113			2	14.3	10	238	[96]

Table 3 (Continued)

Complex	Ligand structure	MW	q	r_1 (mM ⁻¹ s ⁻¹) (20 MHz/298 K)	τ_m (ns) (298 K)	τ_R (ps) (298 K)	Reference
114		557	2	9.5	NA	104	[97]
115		586	2	9.3	NA	116	[97]
116		788	2	NA	19 (320 K)	NA	[98]
117		422	1	9.37 (310 K)	NA	NA	[99]
118		689	2	9.0	16	129	[100]

MW: molecular weight; *: anchoring point; Ph: phenyl ring; NA: not available.

114 and **115**, they have a low water solubility which hinders their clinical applications. Linking the gadolinium complexes to macromolecules or increasing the hydration number increases relaxivity; however, if the water exchange rate is slow, an increase in the inner-sphere water molecules may not have a profound effect on the observed relaxivity. For example, a MS-325 analogue has a slow exchange rate of 4.4×10^5 s⁻¹, and the relaxivity of the HSA adduct is only 22.0 mM⁻¹ s⁻¹ [77]. This illustrates the importance of both the water exchange rate and the hydration number for a high relaxivity, especially for those complexes with macromolecular interactions, which will be discussed in the next session.

3. Pharmacokinetics

The study of the relationship between a protein and its biological function is important in understanding the basis of life and disease. Since the function of proteins is closely related to their conformation, contrast agents that can specially probe the conformation may be an essential tool to reveal in vivo physiochemistry. The interaction of contrast agents with macromolecules slows down the tumbling rate and increases the relaxivity, provided that the water exchange rate and the electronic relaxation are not limiting. The non-covalent interaction is of particular interest because of its better accessibility towards low concentration targets, e.g. cell surface receptors, and fewer toxicological problems [101].

The common administration pathway is intravenous injection (i.v.), hence, the interaction between the contrast agents and HSA

has been extensively studied [56,60,102–108]. HSA is the most abundant protein in blood plasma, with a molecular weight of 66 kDa and a concentration of between 0.53 and 0.75 mM. It has many hydrophobic binding sites, such as the eight sites for fatty acids. The function of HSA is to bind and transport exogenous and endogenous ligands, including fatty acids, metal ions, and pharmaceuticals. Ligands usually bind with the hydrophobic pockets that are formed by different properties of amino acid residues [101,109].

The binding affinity K_A is expressed in Eq. (3.1) [104], and the resulting relaxivity r_1^b , that is the relaxivity of the adducts form between the complex and the macromolecule, for example HSA, can be measured by the proton relaxation enhancement (PRE) method. PRE is based on the titration of the complex against the binding substrate of HSA. The binding of the complexes to HSA influences the τ_R , τ_m , T_{1e} , and T_{1M} of the complexes:

$$K_A = \frac{[\text{GdL} - \text{HSA}]}{[\text{GdL}][\text{nHSA}]} \quad (3.1)$$

The identity of the HSA binding site can be determined through competitive binding assays with known binding substrates, such as ibuprofen, warfarin, bilirubin, linolenic acid, and 1,3,5-triiodobenzoic acid [104]. The ibuprofen and warfarin are ligands that strongly bind to the sub-domains IIA and IIIA of HSA respectively [101].

The r_1^b can be 16 times higher than that of the unbound complex, because of the receptor-induced magnetization enhancement (RIME) effect [110], that increases the τ_R upon macromolecular binding.

HSA binding interaction acts as a valuable model to study the mechanism of binding and relaxivity change for the interaction between a contrast agent and its corresponding protein target. It also helps to unveil the properties that improve the protein–chelate interaction, and more importantly, increase the *in vivo* relaxivity and specificity.

3.1. HSA binding

The three factors govern the strength of HSA binding are the hydrophobicity, electrostatic interaction and stereospecificity. A series of gadolinium complexes that show different degrees of affinity towards HSA are complexes **24–28**, **34** and **35**, **37–41**, **48** and **49**, **66**, **83**, **89–91**.

In general, hydrophobic substituents of an appropriate size [111] are preferred for their better affinity towards HSA. The benzyloxymethyl (BOM) group shows a favourable protein binding. Chelates in the literature contains different number of BOM groups, which are the DOTA, DTPA, and 3,6,10-tri(carboxymethyl)-3,6,10-triazadodecanedioic acid (TTDA) derivatives [89,103,112]. The tetrasubstituted Gd-DOTA(BOM)₄ (complex **41**) was recently reported to have a preferable bovine serum albumin (BSA) affinity, and resulted in a high r_1^b of 57.4 mM^{−1} s^{−1} in plasma. Pendent groups similar to BOM, such as complex **26–28**, bind to the well-defined domains I and II of HSA and have a similar binding affinity with K_A falls in a range of 5900–9300 M^{−1}. The two phenyl rings of complex **66**, which is a MS-325-like (MS-325 is Gadofosveset, VasovistTM as shown in Fig. 4 and has a K_A = 11000 M^{−1}) complex, has a moderate K_A of 4500 M^{−1}. The consecutive phenyl rings of complex **39** and **40** bind to the site II subdomain IIIA of HSA. The triphenyl derivative has the highest affinity (K_A = 9.5 × 10⁴ M^{−1}), due to the strong affinity towards the hydrophobic pockets of HSA. Complex **89** also have favourable HSA binding, the trisubstituted phenyl is ascribed to the strong binding and the K_A is 10100 M^{−1}. Apart from the aromatic functional groups mentioned, a non-aromatic pentylbicyclo[2.2.2]octane of MP-2269, which is negatively charged also strongly binds with HSA [113]. Alternatively, short chain and long chain aliphatic groups have affinities in ascending order [101] because of an increase in hydrophobicity, that is, complex **38** binds stronger than complex **37**.

A negatively charged complex is advantageous for protein interaction when a similar hydrophobicity exists, because the inner surface of the hydrophobic pocket of HSA is positively charged and a negative charge complex is usually preferred [114]. The higher affinity of Gd-DTPA(BOM)₃ [104], with a K_A of 4 × 10⁴ M^{−1}, than that of Gd-DOTA(BOM)₃ is a result of the overall two negative charge on the DTPA derivative, which is independent of the chelates. If the cyclen is rigidified to increase hydrophobicity without a negative charge, the complex is not favourable for protein interaction either, like Gd-PCTP[13] [107]. It has a K_A of 600 M^{−1} and the r_1^b is 45 mM^{−1} s^{−1}. The introduction of a negative charge favours the interaction with the HSA and a high r_1^b . Modifications on Gd-PCTP[12] by adding a benzyl group, such as complex **48**, is not suitable for a high

affinity. Further modification by adding a negative phosphonate group greatly enhances the binding. Complex **49** is analogous to complex **48**, but with a higher HSA affinity of 3300 M^{−1}. This also suggests that the benzyl group is not an appropriate hydrophobic moiety to promote the HSA binding in this system. If the phosphonate group is linked to a benzyl group, the binding affinity is not reinforced. The affinity of complex **35** is three times weaker than complex **34**, i.e. 5400 M^{−1} versus 1800 M^{−1}. The two negative charges on the phenyl ring of complex **50** are too hydrophilic and geometrically unfavourable for binding to the hydrophobic pocket of HSA. In the Gd-DOTP family, which is phosphonate tetrasubstituted cyclen [115], such as Gd-BzDOTP [116] and Gd-DOTPMB [117] have moderate protein affinities of K_A = 3600 and 930 M^{−1}, respectively in the presence of the negatively charged phosphonate group. From these data we may conclude that both the hydrophobicity and the electrostatic interaction are determinants for the HSA affinity of a complex.

In addition, stereospecificity is important in determining the strength of HSA binding. The R- and S- isomers of Gd-EOB-DTPA have different affinities towards of the same binding site on HSA, and the S-isomer has a higher affinity [118]. Since the absence of an influence on the magnetic interaction between the Gd and water molecules, the r_1^b are the same for both isomers. Ideally, the affinity and specificity can be manipulated by choosing a targeting group with an appropriate isomer and a high affinity towards a particular domain.

3.2. Relaxivity of HSA adducts

The observed r_1^b is expected to be close to the theoretical maximum of 100 mM^{−1} s^{−1} for complexes with an inner-sphere water molecule and a fast water exchange rate upon HSA binding. However, the r_1^b is much lower than expected because of the formation of ternary adduct. This is a consequence of the perturbation of the hydration sphere or a substitution of bound water molecules by hard donor groups of proteins, probably the carboxylate or endogenous bidentate anion. When the hydration number decreases, the r_1^b is low, even under the circumstance of the RIME effect that is a lengthened τ_R . As a result, r_1^b , which is mainly outer-sphere and/or second-sphere relaxivity, is confined to protons in proximity of the complex and the hydration sphere of proteins. The inertness towards the formation of ternary adducts increases if the inner-sphere water molecule is protected in the coordination cage, which is located further away from the protein surface. Complexes **39** and **40** are two DOTMA [60] analogues with phenyl rings that show high affinities towards HSA and their relaxivities increase to 35 and 43.5 mM^{−1} s^{−1} accordingly. The water exchange occurs between the hydration layer and the surface of the protein. With respect to their molecular modeling, complex **39** is more embedded and the four acetate arms form a hydrogen bond with Lys414, whereas complex **40** is between Lu387 and Arg410, which is further from the protein surface and only one acetate arm forms a hydrogen bond with Val493. Therefore, the inner-sphere water molecule is not interfered, and its r_1^b is higher than that of complex **39**. The benzyl group at the distal acetate arm of complex **48** cannot shield the

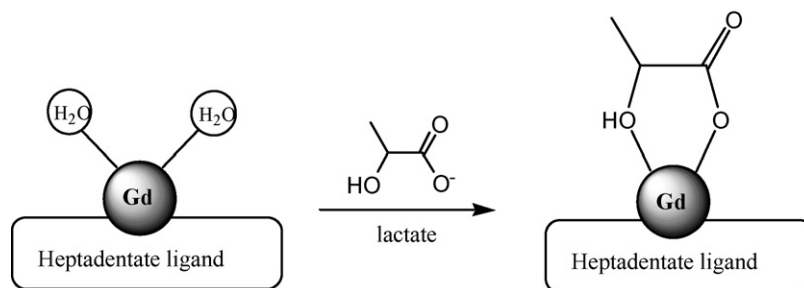


Fig. 2. Schematic diagram of the displacement of inner-sphere water molecules upon lactate bindings, modified from [58].

q from the donor group or the protein surface. The r_1^b is lower than expected and has a value of $40 \text{ mM}^{-1} \text{ s}^{-1}$.

Complexes with more than one inner-sphere water molecules are relatively more reactive towards the formation of a ternary adduct through the carboxylic acid replacement because of a favourable geometric binding site for bidentate ligands, as shown in Fig. 2. The pH dependent relaxivity study shows that complexes **48** and **50**, but not complex **49**, have a relaxivity decrease upon the addition of endogenous bidentate anion like lactate, oxalate and tartrate. This demonstrates that the diaqua complex prompts the formation of a ternary adduct. The r_1^b of complexes **34** and **35** is only $21.0\text{--}24.0 \text{ mM}^{-1} \text{ s}^{-1}$, respectively. The relaxivity stems from the outer-sphere or second-sphere because of the substitution by the carboxylate on HSA or phosphate in the buffer. From the luminescence study of their Eu complexes, it can be seen that there is no involvement of the amino or hydroxyl ligation, that is no serine, threonine, or lysine bounded via side chains, which shows the carboxylate group on protein is probably displacing the inner-sphere water molecule. Complexes **27** and **28** are diaqua complexes, having r_1^b of 10.6 and $12.5 \text{ mM}^{-1} \text{ s}^{-1}$, respectively, due to the formation of ternary adducts. More examples of diaqua gadolinium complexes that favour the formation of ternary adducts are complexes **32**, **33**, **36** and **50**. The observed relaxivities are low and fall into a range of $3.7\text{--}4.0 \text{ mM}^{-1} \text{ s}^{-1}$. They have a slow exchange of lactate at the Gd center. A slow exchange rate is another limiting factor for the attainment of a high r_1^b .

The nuclear magnetic resonance dispersion (NMRD) study of a monoqua Gd complex (**C1**), which is shown in Fig. 3, demonstrates the importance of a fast water exchange rate for an increase in the observed relaxivity upon the HSA binding.

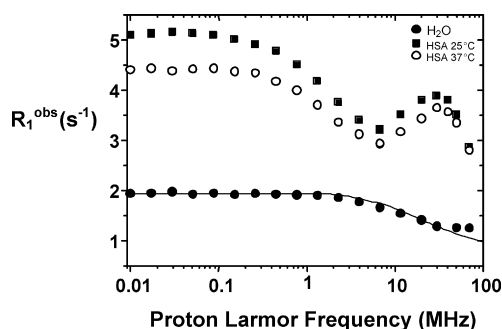


Fig. 3. The NMRD profile of HSA at 120 mg ml^{-1} titrates against **C1** at 0.2 mM at 25 and 37°C , respectively (unpublished data).

The peak at 20 MHz is typical for complexes with an increase in τ_R . The τ_m of **C1** is 930 ns , which represents a slow water exchange rate [119], and the r_1^b is in the lower range. Complexes **90** and **91** are complexes with TTDA skeletons that provide a sterically hindered environment for the bound water molecule. This steric compression facilitates the water exchange, and the increase in τ_R upon the HSA binding leads to a prominent increase in relaxivities (r_1^b is $62\text{--}66 \text{ mM}^{-1} \text{ s}^{-1}$). Complex **89** has a r_1^b of $30.4 \text{ mM}^{-1} \text{ s}^{-1}$, which is less than expected, due to the long reorientation correlation time of the bound water molecule. Complex **66** forms adducts that have a relaxivity of $40 \text{ mM}^{-1} \text{ s}^{-1}$. The reduction in the mobility of solvent molecules in the second coordination sphere limits the relaxivity gain.

Complexes **37** and **38** do not possess inner-sphere water molecules, and the relaxivities of adducts r_1^b are 54 and $77 \text{ mM}^{-1} \text{ s}^{-1}$, respectively. Apart from the electrostatic interaction of the phosphonate groups, they bind to multiple fatty acid binding sites of HSA. The r_1^b of complex **38** depends on the occupancy of the binding sites, that is either the relaxivity of each binding site is different or the relaxivity of a bound site can be changed upon the occupancy of subsequent sites. If the complex is loosely held at weaker sites of HSA; thus, the τ_R of the protein contributes less to the correlation time of the T_{1M} . This explains why the relaxivity of complex **38** decreases as the number of binding sites increases. Thus, the strength of HSA binding and the number of binding sites are not necessarily proportional to the r_1^b . An affinity towards a fast water exchange site on HSA is a method for a high r_1^b .

The relaxometric properties of the complex should be finely adjusted, for example, with a distal paramagnetic center from the binding site, one inner-sphere water molecule and a fast water exchange rate for HSA interaction. In addition, the identity of the site of HSA binding and the internal flexibility of the gadolinium complex can hamper the increase in relaxivity through a macromolecular binding, which is also the perturbation of the hydration sphere or water exchange. This perturbation can be minimized by the multilocus binding [120], which is a strategy to minimize the intramolecular flexibility by increasing the anchoring points on the proteins within a complex.

3.3. Macromolecular structures

Gadolinium complexes form adducts with macromolecules such as β -cyclodextrin [121,122], especially the β -cyclodextrin

multimer, which can interlock the complexes and form oligomers to increase relaxivity. Complexes **48** and **49** have non-covalent interaction towards β -cyclodextrin with K_A 300 M⁻¹ and 95 M⁻¹, and the relaxivity of each adduct is 57 and 46 mM⁻¹ s⁻¹, respectively. For complex **21**, the amine group at the *para* position is responsible for the formation of host–guest adducts with the β -cyclodextrin, and the resulting relaxivity is 8.97 mM⁻¹ s⁻¹.

Avidin–biotin is a golden pair for molecular recognition because of the high affinity between them. Once the contrast agent or the target is conjugated with one of the avidin–biotin partners, they can recognize each other easily [123]. Therefore, a number of biotinylated chelates are prepared to improve drug delivery by providing higher specificity towards the target with avidin conjugation. Complexes **63** and **9** are biotinylated DTPA- and DOTA-like Gd complexes, respectively, which are reported to possibly serve as probes to be conjugated or interact with various biomolecules. Relaxivity upon avidin binding increases to 17.5 mM⁻¹ s⁻¹ ($K_A = 1.7 \times 10^{15}$ M⁻¹) and 4.8 mM⁻¹ s⁻¹ (4:1 = complex:avidin) for the DTPA and DOTA derivatives, respectively.

The micelle and intracellular aggregates also have high relaxivities. Micelle is a spherical aggregate of the complexes in solution with hydrophobic moieties that point towards the center. Complexes **38** and **47** have micellar relaxivities of 18 mM⁻¹ s⁻¹ at above 0.35 mM and 29.2 mM⁻¹ s⁻¹ at a low critical micelle concentration (CMC) of 0.15 mM, respectively. A low CMC means that they can easily aggregate in vitro to enhance relaxivity. The high relaxivity stems from water protons with a long residency time in the vicinity of Gd.

4. Biomedical applications

The in vitro and in vivo properties of contrast agents are of equal importance in the evaluation of the efficacy of contrast agents and the potential to serve specific diagnostic purposes. Sprague–Dawley (SD) rats and Wistar rats are commonly used to elucidate the in vivo performance of contrast agents. The intensity enhancement (IE) of the region of interest at time *t* is expressed by Eq. (4.1):

$$IE = \frac{ROI_t - ROI_0}{ROI_0} \times 100 \quad (4.1)$$

The half lifetime ($t_{1/2}$) can be calculated in Eq. (4.2) by assuming that the uptake and excretion of the contrast agents follows a simplified first-order reaction:

$$IE_t = IE_{\max} \times (1 - e^{-t/t_{1/2}}) \quad (4.2)$$

The IE of clinical EFS agents like Gd-DTPA and Gd-DOTA declines rapidly due to dispersion in the vascular compartments and diffusion in the extracellular space exclusively. Blood-pool, hepatobiliary, renal and molecular agents are widely investigated for specific biomedical uses.

4.1. Blood-pool agents

Magnetic resonance angiography (MRA) is useful in the diagnosis of angiogenesis, which is a pathological state that found in the developments and progressions of several diseases, including cancer, hypertension, rheumatoid arthritis, and diabetic retinopathy [124]. The molecular targets that are related to angiogenesis are the vascular endothelial growth factor (VEGF), which is a key element in sustaining and promoting angiogenesis, and the basic fibroblast growth factor (bFGF). Those that are related to tumor are the $\alpha_v\beta_3$ integrin adhesion receptor, neovasculature specific Tie2 promotor, and hypoxia inducible factor-1 α matrix metalloproteinases (MMPs) [125].

The ESF agents can be administered for MRA studies, but they require precise control of the injection rate and the bolus timing to maximize the contrast. These agents improve the delineation of the arterial morphology in three-dimensional MRA [126,127]. Both Gd-BOPTA and Gd-DO3Abutrol have better mean SNR and CNR in whole body MRA; in particular, Gd-DO3Abutrol is suitable for MR lymphography [128].

The blood-pool agents are classified into albumin-bound and non albumin-bound agents. MS-325 is a well-known small molecular blood-pool agent that has a high HSA affinity and is under Phase III clinical trials [129]. P792 (Gadomitol, VistaremTM) and USPIO are non albumin-bound agents, whereas Gd-BOPTA ($K_A = 490$ M⁻¹) is a weakly albumin-bound agent [130].

The fraction of albumin in the total protein differs by species. For example, rabbits, rats, and mice have a typical value of 50–60% albumin. The sequence is human > pig ~ rabbit > dog ~ rat ~ mouse, which leads to variations in albumin binding among different species, as reported by Eldredge et al. [133]. Therefore, the effect of the relaxivity increases upon the HSA binding may be more prevalent in humans than in rats.

HSA binding agents have a better protection from extravasation into the surrounding tissues, and hence reduce the background and improve contrast. The formation of a HSA-adduct results in a long retention time in the blood stream and a high relaxivity in vitro, as discussed in Section 3.2. However, this relaxivity is measured at fixed concentration of HSA and may not accurately reflect the efficacy of the contrast agent in vivo. Dynamic relaxivity describes the variation in the quantity of bound and free forms and the relaxivity change during the pharmacokinetic profile, which is important in clinical applications. If the interaction with HSA is too strong or too weak, then dynamic relaxivity is not constant [130]. P792 is a non albumin-bound macromolecular complex with molecular weight of 6473 Da and a relaxivity of 42 mM⁻¹ s⁻¹ at 20 MHz and 310 K. Its large molecular size and non-albumin binding property (the relaxivity of the HSA solution is 47.7 mM⁻¹ s⁻¹) [134] minimize its extravasation and excretion. This enables it to have a long intravascular retention time and a minimal change of 5.6% in dynamic relaxivity between the bolus and the post-bolus phases [130]. Although the half-life of MS-325 (a strong albumin-bound agent) is four times longer than that of P792 or Gd-DOTA because of its strong HSA binding and depen-

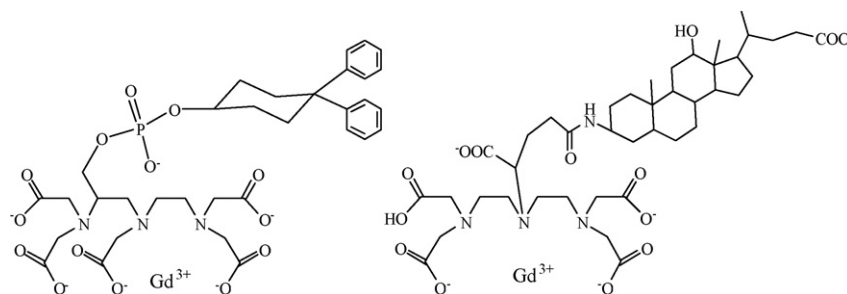


Fig. 4. Structures of blood-pool agents, MS-325 (left) and B22956 (right) [131,132].

dence on albumin concentration [135], it gives a less constant dynamic relaxivity profile than that of P792. The variation in the dynamic relaxivity of MS-325 is $\sim 101\%$ larger than the 29% of Gd-BOPTA (a weak albumin-bound agent) in rabbit [130]. The pharmacokinetics of the blood-pool agents P792 resembles in those of USPIO because of their macromolecular nature. They have a similar intravascular retention and absence of extravasation, thus enhancing the contrast between the vessel and the adjacent tissues. During the bolus phase, the CNR is higher for P792 and USPIO than it is for MS-325, because the majority of the agents are in free form rather than bound form [135].

MS-325 in Fig. 4 strongly binds to HSA at multiple sites. The binding moiety is the diphenylcyclohexyl group, which is bridged to the DTPA via a phosphodiester group [136]. Derivatives of DTPA-linked phosphodiester have been prepared for the *in vivo* study in rats. The addition of phosphodiester increases hydrophilicity and results in a modest increase in HSA binding with respect to Gd-DTPA. Its phosphodiester group is able to interact with the positively charged surface inside the hydrophobic pocket of HSA. These modifications slow down the hepatocellular uptake, reduce the hepatobiliary excretion, and extend the blood half life. Thus, the excretory pathway shifts from the biliary to the renal pathway. Another acyclic DTPA-like agent is the gadocolic acid trisodium salt B22956. Its strong albumin binding helps to reduce its rapid distribution into the extracellular space near the coronary arteries, and it is suitable for coronary angiography [132,137]. In the clinical study, B22956 demonstrates an ability to reveal the vascular properties of tumors after treatment. It shows a decrease in vascular permeability after treatment whereas neither the Gd-HPDO3A nor the (Gd-DTPA)₃₇-albumin do [138], this could be due to the presence of HSA binding and the small size of B22956.

Complexes **11** and **12** show a slow renal wash out kinetics that is altered by homocysteine, and have long blood retention due to HSA binding. Their renal excretory half-life is longer than that of Gd-DTPA. A glucosylated Gd-DTPA has a renal reabsorption mechanism that elongates the vascular retention time. In the presence of a sugar moiety, like β -cellobinoA and β -glucosAmide, these agents show a reduced renal excretion and a slower clearance. The elimination half-life is 24 times longer than that of Gd-DTPA, and has proved not being related to HSA binding and the uptake by erythrocytes [139]. This can be ascribed to the properties of the sugar group, which promotes the recirculation between blood and cells.

The concomitant of blood-pool agents is that they are either non albumin-bound macromolecules, such as polymers or nanoparticles, or a strong albumin-bound agent such as MS-325, or have specific functional groups that can stay longer in the bloodstream such as a glucosylated agent. Thus, the renal or the hepatic excretory pathway is slow down or reduced. Nevertheless, the efficacy of the delivery of contrast agents to cellular targets depends on the HSA interaction, the rate of vascular extravasation, and elimination pathway. The extravasation and elimination of HSA unbound agents show extracellular pharmacokinetics.

4.2. Hepatobiliary and renal agents

The liver allows maximal interaction between blood and liver cells for metabolic and biochemical transformation, especially for xenobiotics. Hepatic contrast agents are applied to improve conspicuity in diagnosis, including the detection of metastases, hepatocellular carcinoma (HCC), and lesion characterization. There are two categories of contrast agents available for the imaging of the liver, which are the small molecular agent and the paramagnetic iron oxide. They have different contrast enhancements because of their different distributions: for example, small molecular agents are not distributed rapidly into the extravascular space and can be taken up by the Kupffer cells, which are the liver macrophages that are directly exposed to the blood stream, or by hepatocytes [140]. Iron oxide particles are taken up by the reticulo-endothelial system (RES) [141].

Gd-BOPTA and Gd-EOB-DTPA are examples of small molecular agents among clinical hepatobiliary agents. They are regarded as the second-generation contrast agents because they provide not only a better anatomical contrast enhancement among the Gd-based clinical agents, but also a better liver-lesion contrast through their specific uptake by the hepatocytes. They have lipophilic pendent arms and a weak HSA-binding [142]. They are negative and are favourably uptaken by the organic anion transporter (OATP) on the hepatocyte or the reticuloendothelial cells, and are involved in the hepatocellular uptake of bilirubin. They are excreted in a non-metabolized form via ATP binding cassette (ABC) proteins that mediate biliary excretion to the bile canaliculi by the glutathione-S-transferase transporter, especially the mrp2 [143,144]. This helps to prevent an accumulation of contrast agents. The duration of the liver IE is 2 h for Gd-BOPTA and Gd-EOB-DTPA [145,146], which is long

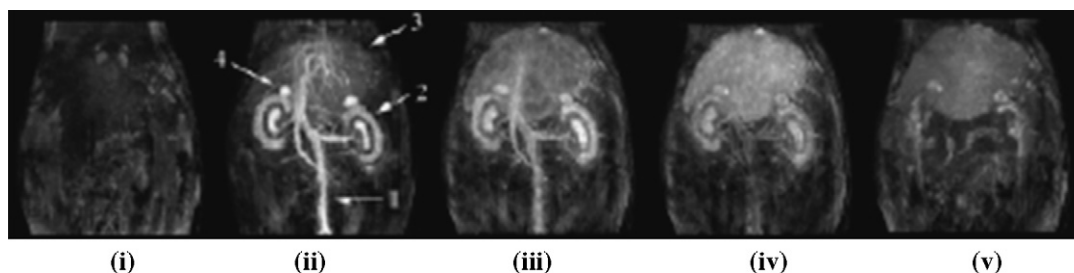


Fig. 5. The abdominal longitudinal section of the rat after an injection of complex **13** at $0.04 \text{ mmol kg}^{-1}$ at p.i.: (i) 0 min, (ii) 5 min, (iii) 30 min, (iv) 100, and (v) 200 min [49].

enough to avoid the necessity of multiple injections during a MRI scan.

Other advantage offered by the uptake of the hepatocytes is that, regardless of the dysfunction of the liver or kidneys the elimination of the agents is efficient. As shown in the animal studies, over 90% of the injected dose of Gd-BOPTA and Gd-DTPA is cleared in the bile duct ligated rat. However, after the ligation of the renal vessel, only Gd-BOPTA can be eliminated via the bile [147].

In a clinical study of Gd-BOPTA, particularly in the delay phase, 7% is taken up by the hepatocytes [146] and excreted in the bile. The high intracellular macromolecule binding is possibly the reason for a long liver parenchyma plateau-like enhancement [148]. It has an exponential dependence on the HSA concentration, whereas Gd-DTPA has a small linear dependency at physiological ranges of serum albumin [149]. Gd-BOPTA has a greater contrast enhancement than both Gd-DTPA and Gd-DOTA in general and for tumor imaging of the vascular system [150,151], central nervous system [152–154] and liver imaging. It may enable grading of HCC because of its specific hepatocyte uptake, active uptake into differentiated carcinoma and delayed elimination [155]. It is suitable for the visualization of other diffuse liver diseases, such as hepatitis and cirrhosis [156,157].

Gd-EOB-DTPA is a well-tolerated hepatobiliary agent and has an increased contrast enhancement and prolonged retention time in the liver, as compared to Gd-DTPA [158]. In clinical study, 50% of the Gd-EOB-DTPA was mainly excreted through bile, and it increased the bile flow significantly [146]. Gd-EOB-DTPA has a significant hepatocellular uptake in normal rat hepatocytes, but not the hepatoma cells. This accumulation is inhibited competitively by bromsulphthalein, which proves its entry is via the OATP [159]. In the case of hepatocellular carcinoma (HCC), the hepatoma cells (HepG2 and Huh7 cells) are lack of OATP and will not take up Gd-EOB-DTPA. Therefore, it gives a homogeneous enhancement of liver parenchyma, and it allows a clear delineation of the bile ducts and small tumors in the liver [159–161]. Gd-EOB-DTPA is safe to apply in the case of hepatitis and cirrhosis, and cholestatic rats [162–164].

New Gd-based contrast agents show hepatic intensity enhancement are the HOPO type agents and the highest IE in the liver is the complex that has a long poly(ethyleneoxy) (PEO) chain [165]. The structure-related selectivity for the liver is better for agents that are analogs to complex **116** with a short PEO chain, because the phenyl group that is responsible for

targeting is dominant instead of the PEO chain. A neutral liver-specific **C1** [119] has shown a 23% increase in the hepatic IE with respect to the clinical hepatobiliary agent Gd-BOPTA in the SD rats. It is hydrophobic and has a weak HSA binding, which allows extravastation and hepatocellular uptake. Agents with bile acid conjugates likely target the hepatocytes [166]. An amide-linked benzyl agent Gd-2,5-BPA-DO3A has a hepatobiliary clearance of 47% in rats, and IE increases significantly in the liver compared to that in blood or extracellular fluids [167].

In rodent studies, IE is usually found in the liver and the kidneys which are major excretory organs. This relates to the hydrophobicity of complexes. For example, complexes **43** has an improved kidney-to-liver ratio [63] in the presence of the azepane ring, and the incorporation of the piperidine ring on DTPA and DOTA enhances the hepatobiliary elimination. An aza-15-crown5 containing agent, complex **13**, has hepatic and renal IE as shown in Fig. 5. The pronounced renal IE may possibly be explained by the sodium ion binding of the crown ether.

The criteria for liver targeting agents may be surmised to a weak HSA binding, hydrophobic targeting group, which can determine the excretory pathway. High hydrophobicity is usually associated with the biliary excretory pathway. In addition, a negatively charged agent can promote the specific hepatocellular uptake via the OATP.

4.3. Molecular agents

Small molecular agents are more readily available for cellular uptake than macromolecular agents. New agents that have various molecular bindings illustrate the possibility for imaging at the molecular level. They can probe disease-related proteins through relaxivity increases upon binding or relaxivity changes under different pathological states. The targeting group and the magnitude of relaxivity increase upon binding are important for the imaging of low concentration receptors or nanomolar targets.

Specificity is important for the small molecular agents to recognize the disease-related proteins. The incorporation of moieties that have high in vitro affinity towards molecular targets and the contrast agent of either DTPA or DOTA is a strategy to improve the specificity. A number of studies that use this strategy has been found in the literature. For example, the asparagines glycine arginine (cNGR) peptide sequence has an affinity towards CD13 which is a protein found in angiogenesis [86]; Evans Blue has an affinity towards endothelium-denuded regions

[168]; a bis(phosphonate) group is preferentially adsorbed on bones that are growing or having pathological changes [52]; sulfonamide ethylene sulfanilamide can bind to the carbonic anhydrase [84]. All these examples provide good specificity, but the percentage change in relaxivity upon binding is limited and has to be increased for clinical application.

The changes in the physiological environment induce changes in the relaxivity of T_1 -agents, such as the presence or the accessibility of enzymes or disease-related proteins. Complex **22** has a β -glucuronidase cleavable bond, the relaxivity increase is possibly due to the gadolinium center being more accessible to water molecules upon enzymatic cleavage. A trilyserine DTPA derivative can be activated by a human carboxypeptidase B thrombin-activable fibrinolysis inhibitor (TAFI) to form a HSA-bound complex. Its relaxivity increases to $12.5\text{--}25.2\text{ mM}^{-1}\text{ s}^{-1}$, and it can be used to detect an enzyme-associated disease state [110].

The erosion and rupture of atherosclerotic plaques are the causes of morbidity and are related to an enzyme (myeloperoxidase MPO), which consumes hydrogen peroxide and generates hypochlorite. On the basis of the findings for Gd(III) serotonin-DOTA [170], Gd(III) 5-hydroxytryptamide-DOTA and Gd(III) tyramide-DOTA, they act as myeloperoxidase-specific substrates that can report the MPO activity. Peroxidases are assumed to mediate the polymerization of these complexes, which amplifies the observed relaxivity [169]. In the presence of hydrogen peroxide, Gd(III) 5-hydroxytryptamide-DOTA has a faster kinetic response than the tyramide derivative with MPO. It demonstrates a high relaxivity increase of 70–100% in the areas that are rich in MPO and is a marker of vascular disease in humans, especially the progression of atherosclerotic plaque from stable to vulnerable [170]. DTPA derivatives (complexes **57–58**) that are endowed with bioactive functional moieties, such as serotonin and tyramine, are prepared for the detection of MPO. Relaxivity increases with an increase in molecular size through the enzyme-induced polymerization and covalent binding of the complex to the macromolecules in the MPO-rich areas [78]. Methods to increase sensitivity, which describes the percentage change of the relaxivity according to the physiological changes, are required before clinical use.

Contrast agents are developed to detect inflammation by probing the selectin. When inflammation takes place, leukocytes and plasma proteins, such as opsonins, antibodies, and complements, are present at the inflammation site. Selectins are a family of cell adhesion proteins that are found during inflammation: E-selectin is on vascular endothelial cells, P-selectin is on platelets and vascular endothelial cells, and L-selectin is on leukocytes. The E-selectin specific contrast agent, Gd-DTPA-B(sLex)A (see complex **61**), is designed to probe inflammation, and the pharmacokinetics are studied in rats [171,172]. This inflammation probe uses the sialyl Lewis^x (sLex) mimetic, which has affinity towards the E-selectin on endothelial cells. It does not interact with albumin, and the relaxivity increase upon the addition of albumin is only 1.3 times that of the free complex. Its relaxivity in rat blood is $4.61\text{ mM}^{-1}\text{ s}^{-1}$ at 60 MHz and 310 K, which is slightly higher than the $4.35\text{ mM}^{-1}\text{ s}^{-1}$ of Gd-DTPA. E-selectin is not found in the normal liver, but in inflammatory liver dis-

eases, such as hepatitis. This agent has a higher affinity towards E-selectin than Sialyl Le^x-PAA-biotin, which shows an increase in the liver uptake, particularly in hepatitis rats. Although its slow elimination may lead to an accumulation in other organs, it demonstrates the ability to image inflamed tissues [172]. The relaxivity gain in this example is small, better strategies have to be employed to maximize the gain. The τ_m of this agent is 259 ns at 310 K [79], hence, structural modification on the chelate to increase the water exchange rate may increase the relaxivity and sensitivity.

Iron oxide-based nano-sized T_2 -agents are alternatives because their compartmentalization gives a significant decrease in T_2 and they can be easily engineered. E-selectin can also be targeted through the use of nanoparticles, such as dextran-coated cross-linked iron oxide (CLIO) nanoparticles [173] and peptide-based CLIO [174]. The CLIO nanoparticles that are conjugated to a high affinity anti-human E-selectin (CD62E) F(ab')₂, thus forming CLIO-F(ab')₂ [173], which may probe different vascular pathologies, such as angiogenesis, atherosclerosis, and inflammation. Human umbilical vein endothelial cells (HUVECs) that are implanted in mice are used to test the specificity of this agent. As the E-selectin is upregulated by VEGF and IL-1 β , the i.v. injection of CLIO-F(ab')₂ shows a hypointensed image under the effect of IL-1 β [175]. These particles in the range of 30–5000 nm are cleared by the RES, particularly Kupffer cells in the liver, and are destroyed by the lysosomes of Kupffer cells. Large particles have prompt macrophage uptake, and the larger the particle is, the more rapid is the clearance by macrophage, which is independent of the surface coating [176].

At the cell level, an intracellular accumulation or extracellular attachment of the contrast agents provides labeled cells for the imaging of their interactions at the cellular level, especially the endothelial progenitor cells (EPC) because of their valuable therapeutic application. Relaxivity increases with concentration and intracellularly in an in vitro NIH 3T3 cell study of complex **10**. An accumulation of agents through an endosomal uptake in the intracellular vesicles leads to localized inhomogeneities of the magnetic field via compartmentalization. Gd-HPDO3A is an EFS agent and has been internalized in rat hepatocarcinoma, and this event is visualized under the confocal microscopy. The paths of intracellular transport are electroporation and pinocytosis [177], and the agent stays in the cellular cytosol and the endosomal vesicles in the perinuclear region [178], respectively. Cells labeled by electroporation are invariably hyperintense relative to those labeled by pinocytosis.

The focus of the iron oxide-based agents is on CLIO, especially the CLIO-Tat, for better cellular delivery. The CLIO-Tat is composed of a small monocrystalline superparamagnetic iron oxide core, which is stabilized by a crosslinked aminated dextran coating and derivatized with a peptide sequence from HIV-1, the transactivator protein. The overall size is approximately 45 nm. The HIV peptide is an efficient vector to carry the iron oxide particles into cells, such as hematopoietic and neural progenitor cells. From the in vitro studies, the cells labeled by CLIO-Tat, for example, CD34+, can be visualized in an MRI scan and assist the development of stem cell therapy [179].

At the gene level, MRI demonstrates the possibility of investigating gene expression. The transferrin (Tf) receptor expression that is either endogenous or genetically induced can be detected using the disulfide CLIO-Tf conjugate [180]. This agent increases the number of Tf per iron oxide particles and minimizes the dosage of iron oxide. The transgene expression, especially the engineered transferrin receptor (ETR), can be monitored both in vitro and in vivo. This is related to an increase in the internalization of the MION-Tf agent, such as in tumors [181]. The HSV-based amplicon vector is incorporated with ETR/Tf-S-S-CLIO, which is a disulfide CLIO, to improve the delivery of the gene to target tissues [182]. These cell and gene studies are successful in vitro, although for most of the cases, a high dosage and better protocol for delivery may be required to detect changes in vivo, especially when iron oxide particles are used because of their low specificity.

Small molecular contrast agents have a dimension of a few Å, which are two orders of magnitude smaller than that of iron oxide particles. Their small size enhances their delivery and diffusion in tissues and cells, such as solid tumors [123] when compared with iron oxide particles. Potential limitations of iron oxide particles for clinical imaging are their limited shelf life and potential immunogenicity under multiple injections. These considerations have hindered their application. The superparamagnetic iron oxide (SPIO) has a prolonged accumulation, particularly in the liver. The T₂ enhancement may lead to problems when the grafted cells are placed in an area with a low intrinsic signal. The enhancement that is based on compartmentalization makes the region sensitive towards an external magnetic field and chaplets can form, which causes deformations along the magnetic field [183]. Small molecules play a crucial role in improving the CLIO for better site-specific or cell-surface targeting [26].

5. Conclusions

Small molecular agents are sensitive towards their vicinity, they have less unforeseeable safety issues and less restriction on diffusion and delivery. This implies that changes in physiological environment that perturb the relaxivity are detectable. The challenges of the frontier chelate design are a fast water exchange site upon Gd coordination and synthons for specific binding; neither one of these criteria hinders the water exchange.

The exchange rate of inner-sphere water molecules of the Gd complex has improved and is a few nanoseconds. This is particularly favourable for an increase in the relaxivity of the complex towards macromolecular binding. The HSA-chelate envisages an ample improvement in the inherited low sensitivity of the T₁-agents. HSA binding is one of the factors that influence the pharmacokinetic profiles, extravascular availability, vascular and hepatic imaging. More knowledge of these structural and relaxometric determinants enables a better design of unique probes to serve different diagnostic purposes.

The availability of a high magnetic field scanner and high sensitive agents allows the imaging at the cell or gene level. The issues in this area are the limited relaxivity gain under different pathologies, difficulty in the delivery of a large amount of contrast agents to low concentration targets, and inefficient

intracellular transport. Innovations in synthetic and conjugation chemistry, contrast agent-protein interaction and drug delivery revolutionize the imaging field by making the imaging of molecular targets in vivo possible.

Acknowledgements

We thank the Hong Kong Research Grants Council for its financial support. Prof. M. Botta at the Dipartimento di Scienze e Tecnologie Avanzate, Università del Piemonte Orientale, and his students for the relaxometric studies and Dr. H. Lei at the Key State Laboratory of Magnetic Resonance and Atomic and Molecular Physics, Wuhan Institute of Physics and Mathematics, Chinese Academy of Sciences, and his students for their assistance in the rat studies are acknowledged.

References

- [1] S. Aime, S.G. Crich, E. Gianolio, G.B. Giovenzana, L. Tei, E. Terreno, *Coord. Chem. Rev.* 250 (2006) 1562.
- [2] A.Y. Louie, M.M. Hüber, E.T. Ahrens, U. Rothbächer, R. Moats, R.E. Jacobs, S.E. Fraser, T.J. Meade, *Nat. Biotechnol.* 18 (2000) 321.
- [3] M. Botta, *Eur. J. Inorg. Chem.* (2000) 399.
- [4] S. Aime, M. Botta, M. Fasano, E. Terreno, *Acc. Chem. Res.* 32 (1999) 941.
- [5] R.A. de Graaf, P.B. Brown, S. McIntyre, T.W. Nixon, K.L. Behar, D.L. Rothman, *Magn. Reson. Med.* 56 (2006) 386.
- [6] R.B. Lauffer, *Chem. Rev.* 87 (1987) 901.
- [7] P. Caravan, J.J. Ellison, T.J. McMurry, R.B. Lauffer, *Chem. Rev.* 99 (1999) 2293.
- [8] S. Aime, M. Botta, M. Fasano, S.G. Crich, E. Terreno, *Coord. Chem. Rev.* 185–186 (1999) 321.
- [9] S. Aime, M. Botta, M. Fasano, E. Terreno, *Chem. Soc. Rev.* 27 (1998) 19.
- [10] P. Caravan, A.V. Astashkin, A.M. Raitsimring, *Inorg. Chem.* 42 (2003) 3972.
- [11] L. Helm, A.E. Merbach, *Chem. Rev.* 105 (2001) 1923.
- [12] H. Kobayashi, S. Kawamoto, S.-K. Jo, H.L. Bryant, M.W. Brechbiel, R.A. Star, *Bioconjug. Chem.* 14 (2003) 388.
- [13] S. Aime, W. Dastru, R. Gobetto, A. Viale, *Org. Biomol. Chem.* 3 (2005) 3948.
- [14] K.A. Deal, R. Motekaitis, A.E. Martell, M.J. Welch, *J. Med. Chem.* 39 (1996) 3096.
- [15] A. Accardo, D. Tesaro, P. Roscigno, E. Gianolio, L. Paduano, G. D'Errico, C. Pedone, G. Morelli, *J. Am. Chem. Soc.* 126 (2004) 3097.
- [16] W.J.M. Mulder, G.J. Strijkers, A.W. Griffioen, L. van Bloois, G. Molema, G. Storm, G.A. Koning, K. Nicolay, *Bioconjug. Chem.* 15 (2004) 799.
- [17] M.F. Tweedle, V.M. Runge, *Gadoteridol. Drugs Future* 17 (1992) 187.
- [18] W.P. Cacheris, S.C. Quay, S.M. Rocklage, *Magn. Reson. Imaging* 8 (1990) 467.
- [19] N.R. Puttagunta, W.A. Gibby, G.T. Smith, *Invest. Radiol* 31 (1996) 739.
- [20] H. Vogler, J. Platzek, G.S. Giampieri, T. Frenzel, H.-J. Weinmann, B. Radüchel, W.-R. Press, *Eur. J. Radiol.* 21 (1995) 1.
- [21] A. Oksendal, P. Hals, *J. Magn. Reson. Imaging* 3 (1993) 157.
- [22] E. Kanal, F.G. Shellock, *Safety Manual on Magnetic Resonance Imaging Contrast Agents*, Lippincott-Raven Healthcare, Cedar Knolls, NJ, 1996.
- [23] V.M. Runge, *Top. Magn. Reson. Imaging* 12 (2001) 309.
- [24] M.F. Bellin, J.A.W. Webb, A.J. Van der Molen, H.S. Thomsen, S.K. Morcos, *Eur. Radiol.* 15 (2005) 1607.
- [25] M.A. Kirchin, V.M. Runge, *Top. Magn. Reson. Imaging* 14 (2003) 426.
- [26] R. Weissleder, K. Kelly, E.Y. Sun, T. Shtatland, L. Josephson, *Nat. Biotechnol.* 23 (2005) 1418.
- [27] M. Bottrill, L. Kwok, N.J. Long, *Chem. Soc. Rev.* 35 (2006) 557.

- [28] D. Parker, H. Puschmann, A.S. Batsanov, K. Senanayake, *Inorg. Chem.* 42 (2003) 8646.
- [29] E. Terreno, P. Boniforte, M. Botta, F. Fedeli, L. Milone, A. Mortillaro, S. Aime, *Eur. J. Inorg. Chem.* (2003) 3530.
- [30] D.H. Powell, O.M. Ni Dhubhghaill, D. Pubanz, L. Helm, Y.S. Lebedev, W. Schlaepfer, A.E. Merbach, *J. Am. Chem. Soc.* 118 (1996) 9333.
- [31] S. Laurent, L. Vander Elst, R.N. Muller, *Contrast Med. Mol. Imaging* 1 (2006) 128.
- [32] K. Adzamlı, M. Periasamy, M. Spiller, S.H. Koenig, *Invest. Radiol.* 34 (1999) 410.
- [33] S. Laurent, F. Botteman, L. Vander Elst, R.N. Muller, *Eur. J. Inorg. Chem.* (2004) 463.
- [34] L. Vander Elst, F. Maton, S. Laurent, F. Seghi, F. Chapelle, R.N. Muller, *Magn. Reson. Med.* 38 (1997) 604.
- [35] L.D. Bari, G. Pintacuda, P. Salvadori, *Eur. J. Inorg. Chem.* (2000) 75.
- [36] M. Woods, S. Aime, M. Botta, J.A.K. Howard, J.M. Moloney, M. Navet, D. Parker, M. Port, O. Rousseaux, *J. Am. Chem. Soc.* 122 (2000) 9781.
- [37] S. Aime, M. Botta, M. Fasano, M.P.M. Marques, C.F.G.C. Geraldes, D. Pubanz, A.E. Merbach, *Inorg. Chem.* 36 (1997) 2059.
- [38] G. Bombieri, R. Artali, *J. Alloys Compd.* 344 (2002) 9.
- [39] M. Woods, Z. Kovacs, S. Zhang, A.D. Sherry, *Angew. Chem. Int. Ed.* 42 (2003) 5889.
- [40] F.A. Dunand, R.S. Dickins, D. Parker, A.E. Merbach, *Chem. Eur. J.* 7 (2001) 5160.
- [41] S. Zhang, Z. Kovacs, S. Burgess, S. Aime, E. Terreno, A.D. Sherry, *Chem. Eur. J.* 7 (2001) 288.
- [42] J. Rudovský, P. Čížler, J. Kotek, P. Hermann, P. Vojtěšek, I. Lukeš, J.A. Peters, L. Vander Elst, R.N. Muller, *Chem. Eur. J.* 11 (2005) 2373.
- [43] A. Congreve, D. Parker, E. Gianolio, M. Botta, *Dalton Trans.* (2004) 1441.
- [44] R. Ruloff, É. Tóth, R. Scopelliti, R. Tripiet, H. Handel, A.E. Merbach, *Chem. Commun.* (2002) 2630.
- [45] P. Caravan, M.T. Greenfield, X. Li, A.D. Sherry, *Inorg. Chem.* 40 (2001) 6580.
- [46] S. Aime, M. Botta, L. Frullano, S.G. Crich, G. Giovenzana, R. Pagliarin, G. Palmisano, F.R. Sirtori, M. Sisti, *J. Med. Chem.* 43 (2000) 4017.
- [47] A. Mishra, J. Pfeuffer, R. Mishra, J. Engelmann, A.K. Mishra, K. Ugurbil, N.K. Logothetis, *Bioconjug. Chem.* 17 (2006) 773.
- [48] N. Raghunand, B. Jagadish, T.P. Trouard, J.-P. Galons, R.J. Gillies, E.A. Mash, *Magn. Reson. Med.* 55 (2006) 1272.
- [49] C. Li, Y.X. Li, G.L. Law, K. Man, W.T. Wong, H. Lei, *Bioconjug. Chem.* 17 (2006) 571.
- [50] J. Rudovský, J. Kotek, P. Hermann, I. Lukeš, V. Mainero, S. Aime, *Org. Biomol. Chem.* 3 (2005) 112.
- [51] S. Aime, M. Botta, G. Cravotto, L. Frullano, G.B. Giovenzana, S.G. Crich, G. Palmisano, M. Sisti, *Helv. Chim. Acta* 88 (2005) 588.
- [52] V. Kubíček, J. Rudovský, J. Kotek, P. Hermann, L. Vander Elst, R.N. Muller, Z.I. Kolar, H.Th. Wolterbeek, J.A. Peters, I. Lukeš, *J. Am. Chem. Soc.* 127 (2005) 16477.
- [53] S.J. Ratnakar, V. Alexander, *Eur. J. Inorg. Chem.* (2005) 3918.
- [54] J.A. Duimstra, F.J. Femia, T.J. Meade, *J. Am. Chem. Soc.* 127 (2005) 12847.
- [55] S. Aime, G. Cravotto, S.G. Crich, G.B. Giovenzana, M. Ferrari, G. Palmisano, M. Sisti, *Tetrahedron Lett.* 43 (2002) 783.
- [56] M. Botta, S. Quici, G. Pozzi, G. Marzanni, R. Pagliarin, S. Barra, S.G. Crich, *Org. Biomol. Chem.* 2 (2004) 570.
- [57] M. Polášek, J. Rudovský, P. Hermann, I. Lukeš, L. Vander Elst, R.N. Muller, *Chem. Commun.* (2004) 2602.
- [58] E. Terreno, M. Botta, P. Boniforte, C. Bracco, L. Milone, B. Mondino, F. Uggeri, S. Aime, *Chem. Eur. J.* 11 (2005) 5531.
- [59] S. Aime, E. Gianolio, E. Terreno, G.B. Giovenzana, R. Pagliarin, M. Sisti, G. Palmisano, M. Botta, D. Parker, *J. Biol. Inorg. Chem.* 5 (2000) 488.
- [60] S. Aime, E. Gianolio, D. Longo, R. Pagliarin, C. Lovazzano, M. Sisti, *ChemBioChem* 6 (2005) 818.
- [61] R. Hovland, A.J. Aasen, J. Klaveness, *Org. Biomol. Chem.* 1 (2003) 1707.
- [62] D.M. Corsi, L. Vander Elst, R.N. Muller, H. van Bekkum, J.A. Peters, *Chem. Eur. J.* 7 (2001) 1383.
- [63] H.-S. Chong, K. Garmestani, L.H. Bryant, D.E. Milenic, T. Overstreet, N. Birch, T. Le, E.D. Brady, M.W. Mrechbiel, *J. Med. Chem.* 49 (2006) 2055.
- [64] K.W.Y. Chan, S. Barra, M. Botta, W.T. Wong, *J. Inorg. Biochem.* 98 (2004) 677.
- [65] R. Hovland, C. Gtegård, A.J. Aasen, J. Klaveness, *Org. Biomol. Chem.* 1 (2003) 644.
- [66] S. Aime, E. Gianolio, D. Corpillo, C. Cavallotti, G. Palmisano, M. Sisti, G.B. Giovenzana, R. Pagliarin, *Helv. Chim. Acta* 86 (2003) 615.
- [67] L. Burai, É. Tóth, H. Bazin, M. Benmelouka, Z. Jászberényi, L. Helm, A.E. Merbach, *Dalton Trans.* (2006) 629.
- [68] J. Rudovský, M. Botta, P. Hermann, A. Koridze, S. Aime, *Dalton Trans.* (2006) 2323.
- [69] T.M. Lee, T.H. Cheng, M.H. Ou, C.A. Chang, G.C. Liu, Y.M. Wang, *Magn. Reson. Chem.* 42 (2004) 329.
- [70] B. Jebasingh, V. Alexander, *Inorg. Chem.* 44 (2005) 9434.
- [71] F. Botteman, G.M. Nicolle, L. Vander Elst, S. Laurent, A.E. Merbach, R.N. Muller, *Eur. J. Inorg. Chem.* (2002) 2686.
- [72] Z. Jászberényi, É. Tóth, T. Kálai, R. Kiraly, L. Burai, E. Brücher, A.E. Merbach, K. Hideg, *Dalton Trans.* (2005) 694.
- [73] S. Laus, R. Ruloff, É. Tóth, A.E. Merbach, *Chem. Eur. J.* 9 (2003) 3555.
- [74] Z. Jászberényi, A. Sour, É. Tóth, M. Benmelouka, A.E. Merbach, *Dalton Trans.* (2005) 2713.
- [75] V.C. Pierre, M. Botta, S. Aime, K.N. Raymond, *J. Am. Chem. Soc.* 128 (2006) 5344.
- [76] C.J. Sunderland, M. Botta, S. Aime, K.N. Raymond, *Inorg. Chem.* 40 (2001) 6746.
- [77] P. Caravan, J.C. Amedio, S.U. Dunham, M.T. Greenfield, N.J. Cloutier, S.A. McDermid, M. Spiller, S.G. Zech, R.J. Looby, A.M. Raitsimring, T.J. McMurphy, R.B. Lauffer, *Chem. Eur. J.* 11 (2005) 5866.
- [78] M. Querol, J.W. Chen, A.A. Bogdanov, *Org. Biomol. Chem.* 4 (2006) 1887.
- [79] S. Laurent, L. Vander Elst, Y. Fu, R.N. Muller, *Bioconjug. Chem.* 15 (2004) 99.
- [80] R. Ruloff, G. van Koten, A.E. Merbach, *Chem. Commun.* (2004) 842.
- [81] S. Langereis, H.-A.T. Kooistra, M.H.P. van Genderen, E.W. Meijer, *Org. Biomol. Chem.* 2 (2004) 1271.
- [82] J. Kotek, P. Lebedušková, P. Hermann, L. Vander Elst, R.N. Muller, C.F.G.C. Geraldes, T. Maschmeyer, I. Lukeš, J.A. Peters, *Chem. Eur. J.* 9 (2003) 5899.
- [83] S. Laurent, L. Vander Elst, S. Houzé, N. Guerit, R.N. Muller, *Helv. Chim. Acta* 83 (2000) 394.
- [84] P.L. Anelli, I. Bertini, M. Fragai, L. Lattuada, C. Luchinat, G. Parigi, *Eur. J. Inorg. Chem.* (2000) 625.
- [85] D.-W. Zhang, Z.-Y. Yang, S.-P. Zhang, R.-D. Yang, *Chem. Pharm. Bull.* 54 (2006) 406.
- [86] A. Dirksen, S. Langereis, B.F.M. de Waal, M.H.P. van Genderen, E.W. Meijer, Q.G. de Lussanet, T.M. Hackeng, *Org. Lett.* 6 (2004) 4857.
- [87] H. Tanaka, Y. Ando, M. Wada, T. Takahashi, *Org. Biomol. Chem.* 3 (2005) 3311.
- [88] T.N. Parac-Vogt, K. Kimpe, S. Laurent, L. Vander Elst, C. Burtea, F. Chen, R.N. Muller, Y. Ni, A. Verbruggen, K. Binnemans, *Chem. Eur. J.* 11 (2005) 3077.
- [89] M.-H. Ou, C.-H. Tu, S.-C. Tsai, W.-T. Lee, G.-C. Liu, Y.-M. Wang, *Inorg. Chem.* 45 (2006) 244.
- [90] T.-H. Cheng, T.-M. Lee, M.-H. Ou, C.-R. Li, G.-C. Liu, Y.-M. Wang, *Helv. Chim. Acta* 85 (2002) 1033.
- [91] T.-H. Cheng, Y.-M. Wang, K.-T. Lin, G.-C. Liu, *J. Chem. Soc. Dalton Trans.* (2001) 3357.
- [92] A. Facchetti, A. Abboto, L. Beverina, S. Bradamante, P. Mariani, C.L. Stern, T.J. Marks, A. Vacca, G.A. Pagani, *Chem. Commun.* (2004) 1770.
- [93] E.P. Mayoral, M. Garcia-Amo, P. López, E. Soriano, S. Cerdán, P. Balles-teros, *Bioorg. Med. Chem.* 11 (2003) 5555.
- [94] C. Platas-Iglesias, M. Mato-Iglesias, K. Djanashvili, R.N. Muller, L.V. Elst, J.A. Peters, A. de Bias, T. Rodriguez-Bias, *Chem. Eur. J.* 10 (2004) 3579.
- [95] S.M. Cohen, J. Xu, E. Radkov, K.N. Raymond, M. Botta, A. Barge, S. Aime, *Inorg. Chem.* 39 (2000) 5747.

- [96] V.C. Pierre, M. Botta, K.N. Raymond, *J. Am. Chem. Soc.* 127 (2005) 504.
- [97] J. Xu, D.G. Churchill, M. Botta, K.N. Raymond, *Inorg. Chem.* 43 (2004) 5492.
- [98] M.K. Thompson, M. Botta, G. Nicolle, L. Helm, S. Aime, A.E. Merbach, K.N. Raymond, *J. Am. Chem. Soc.* 125 (2003) 14274.
- [99] Y. Bretonnière, M. Mazzanti, J. Pécaut, F.A. Dunand, A.E. Merbach, *Chem. Commun.* (2001) 621.
- [100] S. Hajela, M. Botta, S. Giraudo, J. Xu, K.N. Raymond, S. Aime, *J. Am. Chem. Soc.* 122 (2000) 11228.
- [101] T.J. Peters, *All About Albumin: Biochemistry, Genetics and Medical Applications*, Academic Press, San Diego, CA, 1996.
- [102] P. Caravan, N.J. Cloutier, M.T. Greenfield, S.A. McDermid, S.U. Dunham, J.W.M. Bulte, J.C. Amedio, T.J. McMurphy, R.B. Lauffer, *J. Am. Chem. Soc.* 124 (2002) 3152.
- [103] S. Aime, M. Botta, M. Fasano, S.G. Crich, E. Terreno, *J. Biol. Inorg. Chem.* 1 (1996) 312.
- [104] S. Aime, M. Chiaussa, G. Digilio, E. Gianolio, E. Terreno, *J. Biol. Inorg. Chem.* 4 (1999) 766.
- [105] L. Vander Elst, S. Laurent, H.M. Bintoma, R.N. Muller, *MAGMA* 12 (2001) 135.
- [106] R.N. Muller, B. Radüchel, S. Laurent, J. Platzek, C. Piérart, P. Mareski, L. Vander Elst, *Eur. J. Inorg. Chem.* (1999) 1949.
- [107] S. Aime, M. Botta, S.G. Crich, G.B. Giovenzana, R. Pagliarin, M. Piccinini, M. Sisti, E. Terreno, *J. Biol. Inorg. Chem.* 2 (1997) 470.
- [108] N.A. Kratochwil, W. Huber, F. Muller, M. Kansy, P.R. Gerber, *Biochem. Pharmacol.* 64 (2002) 1355.
- [109] D.C. Carter, J.X. Ho, *Adv. Protein Chem.* 45 (1994) 153.
- [110] A.L. Nivorozhkin, A.F. Kolodziej, P. Caravan, M.T. Greenfield, R.B. Lauffer, T.J. McMurphy, *Angew. Chem. Int. Ed.* 40 (2001) 2903.
- [111] A.E. Merbach, É. Tóth, *The Chemistry of Contrast Agents in Medical Magnetic Resonance Imaging*, Wiley, 2001, p. 213.
- [112] F. Uggeri, S. Aime, P. Anelli, M. Botta, M. Brocchetta, C. de Haën, G. Ermondi, M. Grandi, P. Paoli, *Inorg. Chem.* 34 (1995) 633.
- [113] K. Adzamlı, M. Spiller, D. Phys, S.H. Koenig, *Acad. Radiol.* 9 (2002) S11.
- [114] X.M. He, D.C. Carter, *Nature* 358 (1992) 209.
- [115] S. Aime, M. Chiaussa, G. Digilio, E. Gianolio, E. Terreno, *Magn. Reson. Med.* 30 (1993) 583.
- [116] S. Aime, A.S. Batsanov, M. Botta, J.A.K. Howard, D. Parker, K. Senanayake, G. Williams, *Inorg. Chem.* 33 (1994) 4696.
- [117] C.F. Galdes, A.D. Sherry, I. Lazar, A. Miseta, P. Bogner, E. Berenyi, B. Sumegi, G.E. Kiefer, K. McMillan, F. Maton, *Magn. Reson. Med.* 30 (1993) 696.
- [118] L. Vander Elst, F. Chappelle, S. Laurent, R.N. Muller, *J. Biol. Inorg. Chem.* 6 (2001) 196.
- [119] K.W.Y. Chan, W. T. Wong, *US Patent* 60/738,102 (2005).
- [120] Z. Zhang, M.T. Greenfield, M. Spiller, T.J. McMurphy, R.B. Lauffer, P. Caravan, *Angew. Chem. Int. Ed.* 44 (2005) 6766.
- [121] S. Aime, E. Gianolio, E. Terreno, I. Menegotto, C. Bracco, L. Milone, G. Cravotto, *Magn. Reson. Chem.* 41 (2003) 800.
- [122] S. Aime, M. Botta, F. Fedeli, E. Gianolio, E. Terreno, P. Anelli, *Chem. Eur. J.* 24 (2001) 5261.
- [123] D. Artemov, N. Mori, R. Ravi, Z.M. Bhujwalla, *Cancer Res.* 63 (2003) 2723.
- [124] P. Carmeliet, *Nat. Med.* 9 (2003) 653.
- [125] N.G. Costouros, F.E. Diehn, S.K. Libutti, *J. Cell. Biochem. Suppl.* 39 (2002) 72.
- [126] C. Fink, M. Puderbach, S. Ley, F. Risse, T.A. Kuder, M. Bock, J. Thaler, C. Plathow, H.-U. Kauczor, *J. Magn. Reson. Imaging* 22 (2005) 286.
- [127] M. Goyen, C.U. Herborn, F.M. Vogt, K. Kröger, R. Verhagen, F. Yang, S. Bosk, J.F. Debatin, S.G. Ruehm, *J. Magn. Reson. Imaging* 17 (2003) 565.
- [128] C. Fink, M. Bock, F. Kiessling, S. Delorme, *Invest. Radiol.* 37 (2002) 655.
- [129] K. Shamsi, E.K. Yucel, P. Chamberlin, *Invest. Radiol.* 41 (2006) 822.
- [130] M. Port, C. Corot, X. Violas, P. Robert, I. Raynal, G. Gagneur, *Invest. Radiol.* 40 (2005) 565.
- [131] R.B. Lauffer, D.J. Parmelee, S.U. Dunham, H.S. Ouellet, R.P. Dolan, S. Witte, T.J. McMurphy, R.C. Walovitch, *Radiology* 207 (1998) 529.
- [132] C. de Haën, P.L. Anelli, V. Lorusso, A. Morisetti, F. Maggioni, J. Zhen, F. Uggeri, F.M. Cavagna, *Invest. Radiol.* 41 (2006) 279.
- [133] H.B. Eldredge, M. Spiller, J.M. Chasse, M.T. Greenwood, P. Caravan, *Invest. Radiol.* 41 (2006) 229.
- [134] L. Vander Elst, I. Raynal, M. Port, P. Tisnès, R.N. Muller, *Eur. J. Inorg. Chem.* (2005) 1142.
- [135] C. Corot, X. Violas, P. Robert, G. Gagneur, M. Port, *Invest. Radiol.* 38 (2003) 311.
- [136] T.J. McMurphy, D.J. Parmelee, H. Sajiki, D.M. Scott, H.S. Ouellet, R.C. Walovitch, Z. Tyeklar, S. Dumas, P. Bernard, S. Nadler, K. Midelfort, M. Greenfield, J. Troughton, R.B. Lauffer, *J. Med. Chem.* 45 (2002) 3465.
- [137] J. Zheng, D. Li, F. Maggioni, D. Abendschein, O. Simonetti, G. Laub, J.P. Finn, R.J. Gropler, F.M. Cavagna, *Invest. Radiol.* 40 (2005) 604.
- [138] P. Marzola, S. Ramponi, E. Nicolato, E. Lovati, M. Sandri, L. Calderan, C. Crescimanno, F. Merigo, A. Sbarbati, A. Grotti, S. Vultaggio, F. Cavagna, V. Lorusso, F. Osculati, *Invest. Radiol.* 40 (2005) 421.
- [139] C. Burtea, S. Laurent, J.-M. Colet, L. Vander Elst, R.N. Muller, *Invest. Radiol.* 38 (2003) 320.
- [140] J. Petersein, A. Spinazzi, A. Giovagnoni, P. Soyer, F. Terrier, R. Lencioni, C. Bartolozzi, L. Grazioli, A. Chiesa, R. Manfredi, P. Marano, E.L.V. van Meerten, J.L. Bloem, C. Petre, G. Marchal, A. Greco, M.T. McNamara, A. Heuck, M. Reiser, M. Laniado, C. Claussen, H.E. Daldrup, E. Rummeny, M.A. Kirchin, G. Pirovano, B. Hamm, *Radiology* 215 (2000) 727.
- [141] P. Reimer, T. Balzer, *Eur. Radiol.* 13 (2003) 1266.
- [142] F.M. Cavagna, F. Maggioni, P.M. Castelli, M. Dapra, L.G. Imperatori, V. Lorusso, B.G. Jenkins, *Invest. Radiol.* 32 (1997) 780.
- [143] L. Pascolo, S. Petrovic, F. Cupelli, C.V. Bruschi, P.L. Anelli, V. Lorusso, M. Visigalli, F. Uggeri, C. Tiribelli, *Biochem. Biophys. Res. Commun.* 282 (2001) 60.
- [144] V. Lorusso, L. Pascolo, C. Ferneti, M. Visigalli, P. Anelli, C. Tiribelli, *Biochem. Biophys. Res. Commun.* 293 (2002) 100.
- [145] B. Hamm, T. Staks, A. Mühler, M. Bollow, M. Taupitz, T. Frenzel, K.-J. Wolf, H.-J. Weinmann, *Radiology* 195 (1995) 785.
- [146] O. Clément, N. Siauve, M. Lewin, E. de Kerviler, C.-A. Cuénod, G. Frija, *Biomed. Pharmacother.* 52 (1998) 51.
- [147] C. de Haën, V. Lorusso, F. Luzzani, P. Tirone, *Acad. Radiol.* 2 (1995) 232.
- [148] W. Schima, S. Saini, J. Petersein, R. Weissleder, M. Harisinghani, W.M. Smith, P.F. Hahn, *J. Magn. Reson. Imaging* 10 (1999) 80.
- [149] F.L. Giesel, H. von, T. Kobligk, I.D. Wilkinson, P. Siegler, C.-W. von der Lieth, M. Frank, K.P. Lodemann, M. Essig, *Invest. Radiol.* 41 (2006) 222.
- [150] R. Wytenbach, S. Gianella, M. Alerei, A. Braghetti, L. Cozzi, A. Gallino, *Radiology* 227 (2003) 261.
- [151] M.V. Knopp, F.L. Giesel, H. von Tengg-Kobligk, J. Radeleff, M. Requardt, M.A. Kirchin, H.R. Hentrich, *J. Magn. Reson. Imaging* 17 (2003) 694.
- [152] M.V. Knopp, V.M. Runge, M. Essig, M. Hartman, O. Jansen, M.A. Kirchin, A. Moeller, A.M. Seeberg, K.P. Lodemann, *Radiology* 230 (2004) 55.
- [153] C. Colosimo, M.V. Knopp, X. Barreau, E. Gérardin, M.A. Kirchin, F. Guézénec, K.P. Lodemann, *Neuroradiology* 46 (2004) 655.
- [154] V.M. Runge, J. Biswas, B.J. Wintersperger, S.S. Baumann, C.B. Jackson, C.U. Herborn, T. Patel, *Invest. Radiol.* 41 (2006) 244.
- [155] R. Kuwatsuru, M. Kadoya, K. Ohtomo, A. Tanimoto, S. Hirohashi, T. Murakami, Y. Tanaka, K. Yoshikawa, H. Katayama, *Invest. Radiol.* 36 (2001) 632.
- [156] P. Marzola, F. Maggioni, E. Vicinanza, M. Dapra, F.M. Cavagna, *J. Magn. Reson. Imaging* 7 (1997) 147.
- [157] B.E. Davies, M.A. Kirchin, K. Bensel, V. Lorusso, A. Davies, J.R. Parker, N.D. Lafrance, *Invest. Radiol.* 37 (2002) 299.
- [158] R. Hammerstingl, S. Zangos, W. Schwarz, T. Rosen, W.-O. Bechstein, T. Balzer, T.J. Vogl, *Acad. Radiol.* 9 (2002) S119.
- [159] M. Lewin, O. Clément, P.B. Valladier, L. Tran, C.-A. Cuénod, N. Siauve, G. Frija, *Invest. Radiol.* 36 (2001) 9.

- [160] G.S. Giampieri, H.S. Willich, W.-R. Press, C. Negishi, H.-J. Weinmann, *Radiology* 183 (1992) 59.
- [161] G. Marchal, X. Zhang, Y. Ni, P. Vanhecke, J. Yu, A.L. Baert, *Magn. Reson. Imaging* 11 (1993) 665.
- [162] A. Muhler, O. Clement, M. Saeed, J.R. Lake, D.P. Stites, Y. Berthezene, R.C. Brasch, *Invest. Radiol.* 28 (1993) 26.
- [163] N. Kato, M. Takahashi, S. Ihara, T. Tsujimoto, T. Miyazawa, *Acad. Radiol.* 5 (1998) S83.
- [164] O. Clément, A. Mühler, V. Vexler, Y. Berthezene, R.C. Brasch, *Invest. Radiol.* 27 (1992) 612.
- [165] M.K. Thompson, B. Misselwitz, L.S. Tso, D.M.J. Doble, H.S. Willich, K.N. Raymond, *J. Med. Chem.* 48 (2005) 3874.
- [166] P.L. Anelli, L. Lattuada, V. Lorusso, G. Lux, A. Morisetti, P. Morosini, M. Serletti, F. Uggeri, *J. Med. Chem.* 47 (2004) 3629.
- [167] E.R. Marinelli, R. Neubeck, B. Song, T. Wagler, R.S. Ranganathan, K. Sukumaran, P.W. Wedeking, A. Nunn, V.M. Runge, M.F. Tweedle, *Invest. Radiol.* 35 (2000) 8.
- [168] T. Yamamoto, K. Ikuta, K. Oi, K. Abe, T. Uwatoku, F. Hyodo, M. Murata, N. Shigetani, K. Yoshimitsu, H. Shimokawa, H. Utsumi, Y. Katayama, *Bioorg. Med. Chem. Lett.* 14 (2004) 2787.
- [169] A. Bogdanov Jr., L. Matuszewski, C. Bremer, A. Petrovsky, R. Weissleder, *Mol. Imaging* 1 (2002) 16.
- [170] J.W. Chen, W. Pham, R. Weissleder, A. Bogdanov, *Magn. Reson. Med.* 52 (2004) 1021.
- [171] Y. Fu, S. Laurent, R.N. Muller, *Eur. J. Org. Chem.* (2002) 3966.
- [172] S. Boutry, C. Burtea, S. Laurent, G. Tousseau, L. Vander Elst, R.N. Muller, *Magn. Reson. Med.* 53 (2005) 800.
- [173] H.W. Kang, L. Josephson, A. Petrovsky, R. Weissleder, A. Bogdanoy, *Bioconjug. Chem.* 13 (2002) 122.
- [174] M. Funovics, X. Montet, F. Reynolds, R. Weissleder, L. Josephson, *Neoplasia* 7 (2005) 904.
- [175] H.W. Kang, D. Torres, L. Wald, R. Weissleder, A.A. Bogdanov, *Lab. Invest.* 86 (2006) 599.
- [176] K.C. Briley-Saebo, L.O. Johansson, S.O. Hustvedt, A.G. Haldorsen, A. Bjørnerud, Z.A. Fayad, H.K. Ahlstrom, *Invest. Radiol.* 41 (2006) 560.
- [177] E. Terreno, S.G. Crich, S. Belfiore, L. Biancone, C. Cabella, G. Esposito, A.D. Manazza, S. Aime, *Magn. Reson. Med.* 55 (2006) 491.
- [178] S.G. Crich, L. Biancone, V. Cantaluppi, D. Duò, G. Esposito, S. Russo, G. Camussi, S. Aime, *Magn. Reson. Med.* 51 (2004) 938.
- [179] M. Lewin, N. Carlesso, C.-H. Tung, X.-W. Tang, D. Cory, D.T. Scadden, R. Weissleder, *Nat. Biotechnol.* 18 (2000) 410.
- [180] D. Högemann, L. Josephson, R. Weissleder, J.P. Babilion, *Bioconjug. Chem.* 11 (2000) 941.
- [181] R. Weissleder, A. Moore, U. Mahmood, R. Bhorade, H. Benveniste, E.A. Chiocca, J.P. Babilion, *Nat. Med.* 6 (2000) 351.
- [182] T. Ichikawa, D. Högemann, Y. Saeki, E. Tyminski, K. Terada, R. Weissleder, E.A. Chiocca, J.P. Babilion, *Neoplasia* 4 (2002) 523.
- [183] C. Wilhelm, A. Cebers, J.C. Bacri, F. Gazeau, *Eur. Biophys. J.* 32 (2003) 655.